Check for updates

JGR Biogeosciences

RESEARCH ARTICLE
10.1029/2026JG010127

Coordinated Leaf Trait Acclimation Reduces Simulated Global Photosynthesis Sensitivity to Elevated CO_2 in a Land Surface Model

Chenyu Bian[1,2], Erqian Cui[1], Xuanze Zhang[3], Ying-Ping Wang[4], Yiqi Luo[5], and Jianyang Xia[1]

[1]Research Center for Global Change and Ecological Forecasting, Institute of Eco-Chongming, School of Ecological and Environmental Sciences, East China Normal University, Shanghai, China, [2]Department of Biological and Environmental Engineering, Cornell University, Ithaca, NY, USA, [3]Key Laboratory of Water Cycle and Related Land Surface Processes, Institute of Geographical Sciences and Natural Resources Research, Chinese Academy of Sciences, Beijing, China, [4]CSIRO Environment, Clayton South, VIC, Australia, [5]School of Integrative Plant Science, Cornell University, Ithaca, NY, USA

Abstract The CO_2 fertilization effect, quantified as the sensitivity of global photosynthesis to elevated atmospheric CO_2 concentration (β_{GPP}), is likely overestimated in the current generation of Earth system models. An emerging hypothesis is that coordinated acclimation of leaf structural and physiological traits, represented by specific leaf area (SLA) and area-based leaf nitrogen content (N_a), can reduce photosynthetic sensitivity to elevated CO_2, thereby lowering simulated β_{GPP} in these models. This study integrated experimental data with the Community Atmosphere Biosphere Land Exchange (CABLE) model to investigate how coordinated trait acclimation modifies β_{GPP}. The global meta-analysis revealed that elevated CO_2 decreases the intercept of the relationship between SLA and N_a. Incorporating this relationship into the CABLE model reduced simulated β_{GPP} by 7.1% globally, with substantial spatial variation. The regional variation was primarily driven by spatial differences in aridity (48.2%), leaf area index (41.4%), and maximum carboxylation rate (v_{cmax}, 5.5%), with the coordinated trait effect on gross primary production decreasing along the aridity gradient. Our findings identify coordinated leaf trait acclimation as an important mechanism for refining simulated β_{GPP}, highlighting the need for trait-based mechanisms in Earth system models to better predict ecosystem responses to global change.

Plain Language Summary Plants absorb the largest carbon flux from the atmosphere into terrestrial ecosystems through photosynthesis. However, the sensitivity of global photosynthesis to rising atmospheric CO_2 may be overestimated in current assessments reported by the Global Carbon Project. One possible hypothesis is that plants can adjust their leaf structural and physiological traits under elevated CO_2, which could reduce this response. In this study, we combined experimental observations with a global land surface model (CABLE) to evaluate how acclimation through coordinated changes in leaf traits influences the simulated sensitivity of global photosynthesis to rising CO_2. We analyzed data from 134 elevated CO_2 experiments and found that elevated CO_2 decreases the intercept of the relationship between specific leaf area and nitrogen content. Incorporating this relationship into the CABLE model reduced the simulated global photosynthesis response to rising CO_2 by nearly 7%. This spatial variation was largely regulated by changes in aridity and canopy structure. These findings suggest that plant trait acclimation provides an important mechanism for regulating simulated global carbon uptake and should be represented in land surface models to improve predictions of future climate-carbon feedback.

Key Points:

- The Community Atmosphere Biosphere Land Exchange model simulations suggest that coordinated acclimation of SLA-leaf N reduces modeled CO_2 fertilization of global photosynthesis
- Incorporating observed trait relationships reduced simulated β_{GPP} by ~7% and revealed strong spatial variation
- The changes in aridity and canopy structure regulate the magnitude of trait-mediated reductions in CO_2 fertilization

Supporting Information:

Supporting Information may be found in the online version of this article.

Correspondence to:

J. Xia,
jyxia@des.ecnu.edu.cn

Citation:

Bian, C., Cui, E., Zhang, X., Wang, Y.-P., Luo, Y., & Xia, J. (2026). Coordinated leaf trait acclimation reduces simulated global photosynthesis sensitivity to elevated CO_2 in a land surface model. *Journal of Geophysical Research: Biogeosciences*, *131*, e2026JG010127. https://doi.org/10.1029/2026JG010127

Received 4 JUN 2026
Accepted 19 SEP 2026

Author Contributions:

Conceptualization: Chenyu Bian, Jianyang Xia
Data curation: Erqian Cui
Formal analysis: Chenyu Bian
Funding acquisition: Jianyang Xia
Supervision: Jianyang Xia
Visualization: Chenyu Bian
Writing – original draft: Chenyu Bian
Writing – review & editing: Chenyu Bian, Erqian Cui, Xuanze Zhang, Ying-Ping Wang, Yiqi Luo, Jianyang Xia

© 2026 American Geophysical Union. All rights reserved, including rights for text and data mining and training of artificial intelligence technologies or similar technologies.

1. Introduction

Projections of future photosynthesis responses to rising atmospheric carbon dioxide (CO_2) are highly uncertain across Earth System Models (Friedlingstein et al., 2014; Keenan et al., 2023; Piao et al., 2013), reflecting a limited understanding of carbon-concentration feedback. Recent evidence indicates that the global net land carbon (C) sink is nearly half of that reported by the Global Carbon Project, suggesting a weaker land C sink than previously estimated (Randerson et al., 2025). As the largest C flux between the atmosphere and biosphere (Ryu et al., 2019), plant photosynthesis is primarily determined by leaf structural (i.e., specific leaf area [SLA] or canopy leaf area index [LAI]) and biochemical traits (Ainsworth & Rogers, 2007; Cui et al., 2023; Luo et al., 1994; Reich, 2012). Specifically, extensive observational evidence shows that SLA (the light-capturing surface area per unit leaf

mass) and leaf nitrogen content (N_a, the intensity of nitrogen investment per unit leaf area) are the most critical traits explaining variations in photosynthetic productivity (Dong et al., 2017; Reich, 2012). Plant photosynthetic trait responses to rising CO_2 concentrations, called leaf trait acclimation to CO_2, have been widely studied (Pastore et al., 2019; Smith & Dukes, 2013). Previous studies have demonstrated that elevated CO_2 reduces SLA and N_a (Ainsworth & Long, 2005; Blackman et al., 2016; Lee et al., 2011) while maintaining a robust trade-off relationship between SLA and N_a under elevated CO_2 (Cui et al., 2020). These coordinated trait responses provide a plausible mechanism for modulating simulated terrestrial C uptake and may partly explain why current models overestimate land C sinks. Therefore, understanding how coordinated trait acclimation responds to elevated CO_2 may help explain the weaker land C sink and advance our understanding of carbon-concentration feedback.

Plant photosynthesis typically depends on leaf nitrogen (N) levels (Evans, 1989; Peterson et al., 1999), with the relationship between photosynthesis and leaf N being modulated by leaf structure (Reich et al., 1998). Experimental evidence indicates that elevated CO_2 can reduce the N cost associated with light-harvesting and carbon fixation for Rubisco synthesis (Sage, 1990). By reallocating N from Rubisco to other plant tissues, plants enhance their nitrogen-use efficiency under elevated CO_2 (Bassiouni et al., 2025; Smith et al., 2024). However, most process-based land surface models fail to accurately simulate the response of leaf N content to rising atmospheric CO_2 (Davies-Barnard et al., 2020; Zaehle et al., 2014). On the one hand, these models often fail to account for the reduced leaf N requirements under elevated CO_2 (Smith & Dukes, 2013; Smith et al., 2024), leading to an overestimation of plant N demand and limitation. This, in turn, results in an underestimation of ecosystem photosynthetic productivity. On the other hand, a previous data-model intercomparison study revealed that models tend to overestimate the nitrogen-use efficiency response to elevated CO_2 (Zaehle et al., 2014). This bias suggests that models may underestimate the effective strength of N limitations, leading to an overestimation of photosynthetic productivity under elevated CO_2. Overall, projections of plant photosynthetic responses to elevated CO_2 remain highly uncertain and are strongly influenced by model representations of leaf N content (Ainsworth & Long, 2005).

Another key aspect of leaf trait acclimation is the adjustment of leaf structure (Ainsworth & Long, 2005). Variation in leaf structure, commonly represented by SLA, which quantifies the leaf area per unit of dry mass invested, has been identified as a critical factor in regulating the relationship between photosynthesis and leaf N content (Reich et al., 1998). Field data have demonstrated a positive correlation between net photosynthetic capacity and SLA across various vegetation functional types, including forbs, deciduous species, and evergreens, at any given leaf N concentration (Reich et al., 1998). Elevated CO_2 enhances carbohydrate storage and accumulation of structural compounds (Luo et al., 1994), reducing the leaf area constructed per unit of dry mass invested. Therefore, SLA typically decreases with increasing leaf thickness under elevated CO_2 concentrations. Land surface models generally use SLA to predict LAI (Bian & Xia, 2023; De Kauwe et al., 2014), which is then upscaled to estimate photosynthetic productivity from leaf to canopy level (Wang & Leuning, 1998). However, most models assume a constant SLA for each plant functional type, neglecting changes in SLA induced by elevated CO_2 (De Kauwe et al., 2014; Medlyn et al., 2015). This limitation inevitably biases the photosynthetic productivity simulations, while the related impact assessment is chronically lacking.

The negative relationship between SLA and leaf N content highlights a fundamental trade-off in plant strategy: maximizing light capture area versus optimizing photosynthetic capacity per unit area. This relationship has been extensively studied across both inter- and intraspecies variations (Zhou et al., 2022). Specifically, quick-return species, which invest less dry mass per unit area, tend to exhibit higher SLA (accompanied by lower N_a) and higher mass-based leaf nitrogen content (N_m), whereas slow-return species display the opposite pattern (Reich et al., 1997; Wright et al., 2004). Previous studies demonstrate that these leaf traits are regulated by water availability (Nardini et al., 2012; Rosas et al., 2019), subsequently affecting the photosynthetic response to elevated CO_2. Specifically, plants in humid regions are associated with a fast resource-acquisition strategy, while those in arid areas tend to support a conservative strategy for drought tolerance (Rosas et al., 2019; Wright, Reich, Cornelissen, Falster, Groom, et al., 2005). Trait-trait correlations are increasingly recognized as a more practical approach than assigning a constant average trait value in global vegetation models (Wang et al., 2012; Wright et al., 2004). Therefore, incorporating trait-based information into dynamic global vegetation models (Harper et al., 2016; Van Bodegom et al., 2012) has proven to be a valuable approach for constraining variations in vegetation photosynthetic productivity (Lu et al., 2017; Wang et al., 2012, 2017). Furthermore, existing studies have shown that the SLA-N_a trade-off remains robust under elevated CO_2 conditions (Cui et al., 2020). However,

21698961, 2026, 11, Downloaded from https://agupubs.onlinelibrary.wiley.com/doi/10.1029/2026JG010127 by Cornell University, Wiley Online Library on [06/11/2026]. See the Terms and Conditions (https://onlinelibrary.wiley.com/terms-and-conditions) on Wiley Online Library for rules of use; OA articles are governed by the applicable Creative Commons License

how coordinated trait acclimation influences photosynthetic sensitivity to elevated CO_2 globally remains poorly understood.

This study aims to quantify the impacts of coordinated trait acclimation on simulated photosynthetic sensitivity to elevated CO_2 by integrating experimental data with modeling simulations. First, we analyzed the effect of elevated CO_2 on the bivariate correlation between SLA and N_a using a meta-analysis of compiled data sets from 134 elevated CO_2 experiments worldwide. Subsequently, we incorporated the coordinated trait relationship identified in these experiments into the Australian CABLE model. A series of factorial simulations was conducted to assess the effects of coordinated trait acclimation on simulated photosynthetic sensitivity to elevated CO_2. Finally, we identified the dominant factors driving spatial variations in the impact of coordinated acclimation across global and regional climate zones. This study combines experimental data with model simulations to bridge leaf-level trait responses and ecosystem-scale C cycling processes (Figure 1), providing a model-based assessment of how plant traits regulate carbon-concentration feedback.

2. Methods

2.1. Data Sets of eCO_2 Experiments

Leaf trait data sets were obtained from Cui et al. (2020) and collected through a literature review. These data sets reported changes in leaf economic traits, including SLA ($cm^2\ g^{-1}$), area-based (N_a, $g\ m^{-2}$) and mass-based leaf nitrogen content (N_m, %), and mass-based net photosynthetic rate (A_m, $nmol\ g^{-1}\ s^{-1}$), in response to major global environmental change factors such as elevated CO_2 (eCO_2), warming, drought, and nitrogen addition. To explore the coordinated trait acclimation effect on the carbon-concentration feedback, only SLA and leaf nitrogen content (N_a and N_m) data from the experiments of elevated CO_2 were used (Figure 2a). Overall, the compiled data set includes 192 plant species from 134 studies. We chose to use N_a rather than N_m because N_a is widely used to calculate v_{cmax} in most land surface models (Rogers, 2014; Table S1 in Supporting Information S1) and in this study (Equation 8), where the maximum carboxylation rate is linked to leaf nitrogen per unit leaf area and thereby directly influences gross primary production (GPP). When N_a ($g\ m^{-2}$) were not reported in the original literature, they were derived from N_m (%) using the following equation:

$$N_a = N_m/\mathrm{SLA} \tag{1}$$

where SLA is the specific leaf area (in units of $m^2\ g^{-1}$).

The meta-analysis followed the techniques described by Hedges et al. (1999) using Metawin 2.0. The response of leaf traits to eCO_2 was estimated using the natural log-transformed response ratio (RR):

$$\ln\mathrm{RR} = \ln(X_e/X_a) \tag{2}$$

where X_a and X_e are the average values of leaf traits under the ambient CO_2 (aCO_2) and eCO_2, respectively. The variance (v) was estimated by

$$v = \left(\frac{s.d_a^2}{n_a X_a^2} + \frac{s.d_e^2}{n_e X_e^2}\right) \tag{3}$$

where $s.d_a$ and $s.d_e$ are the standard deviations of leaf traits under aCO_2 and eCO_2, n_a and n_e are the sample sizes of X_a and X_e. Then, the weighted response ratio (RR_{++}) of leaf traits to eCO_2 was calculated based on a mixed-effects model based on the following equation:

$$\mathrm{RR}_{++} = \frac{\sum_{i=1}^{m}\sum_{j=1}^{n} w_{ij}\mathrm{RR}_{ij}}{\sum_{i=1}^{m}\sum_{j=1}^{n} w_{ij}} \tag{4}$$

where w is the weight of each RR, and it is calculated as the reciprocal of its variance ($w = 1/v$). The symbols m and n represent the number of groups and comparisons, respectively. The standard error was calculated as follows:

19448961, 2026, 11, Downloaded from https://agupubs.onlinelibrary.wiley.com/doi/10.1029/2026JG010127 by Cornell University, Wiley Online Library on [06/11/2026]. See the Terms and Conditions (https://onlinelibrary.wiley.com/terms-and-conditions) on Wiley Online Library for rules of use; OA articles are governed by the applicable Creative Commons License

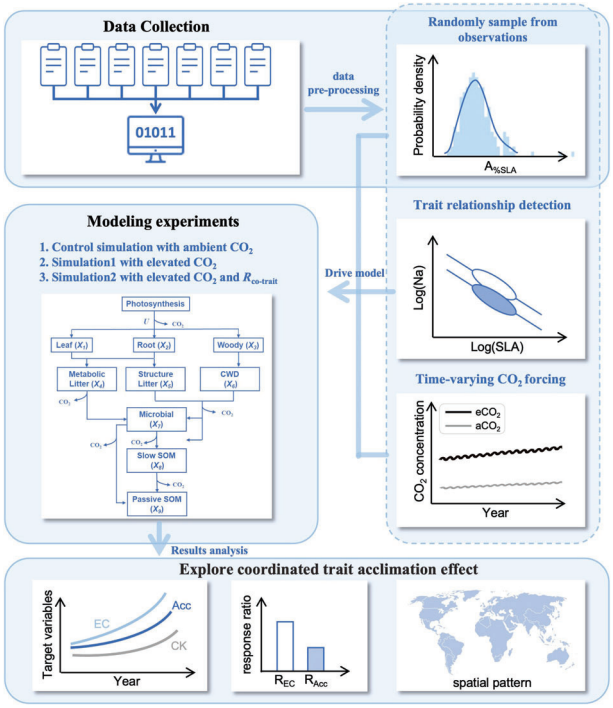


Figure 1. Conceptual framework illustrating the effect of coordinated trait acclimation under elevated CO_2. The framework includes the following steps: first, observational trait data sets were compiled and pre-processed; then, random sampling was applied to generate inputs for subsequent modeling experiments to explore coordinated trait acclimation effects.

$$S(\mathrm{RR}_{++}) = \sqrt{\frac{1}{\sum_{i=1}^{m}\sum_{j=1}^{n} w_{ij}}} \tag{5}$$

21698961, 2026, 11, Downloaded from https://agupubs.onlinelibrary.wiley.com/doi/10.1029/2026JG010127 by Cornell University, Wiley Online Library on [06/11/2026]. See the Terms and Conditions (https://onlinelibrary.wiley.com/terms-and-conditions) on Wiley Online Library for rules of use; OA articles are governed by the applicable Creative Commons License

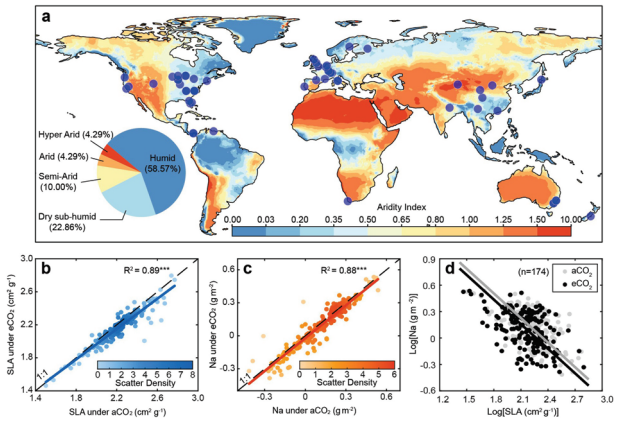


Figure 2. Coordinated leaf trait acclimation between specific leaf area and area-based leaf nitrogen content in log-log scale. a, Global distribution of study sites under elevated CO_2 levels in the meta-analysis. Background colors show the annual mean aridity index from 1970 to 2000, which comes from the Global Aridity Index data sets (v3). Five climate regions are classified based on the Aridity Index values (UNEP, 1997). The lower-left panel shows the proportion of study sites in each climate region. b, The scatter density plot shows the specific leaf area under ambient CO_2 (aCO_2) versus elevated CO_2 (eCO_2). c, Same as b but for the area-based leaf nitrogen content (N_a). The colors in the panels b and c represent the scatter density. The scatter density is estimated based on the "kernel" function. The regressed lines of both panels b and c are significantly different from the 1:1 line based on the *F*-test. d, Coordinated leaf trait relationship between SLA and N_a under aCO_2 and eCO_2, respectively. The regression lines are estimated based on the standardized major axis (SMA) regression, with gray indicating the results under aCO_2 and black representing eCO_2. The regression line under eCO_2 was significantly different from that under aCO_2 according to the SMA analogue of standard ANCOVA. The number of observations is shown on the left side of the legend.

Then, the 95% confidence interval (95% CI) was calculated as $RR_{++} \pm 1.96\ S(RR_{++})$. The response was significant when the 95% CI did not overlap with zero. The percentage change of a variable was calculated as

$$A = [\exp(RR_{++}) - 1] \times 100\% \quad (6)$$

The bivariate trait relationship between SLA and N_a was quantified using standardized major axis (SMA) regression under aCO_2 and eCO_2 conditions. The SMA fit represents the line that aligns with the major axis of the data set, minimizing the sum of squared deviations in both the X and Y dimensions simultaneously. This approach is widely used for fitting trait relationships (Anderegg et al., 2021; Cui et al., 2020; Wright, Reich, Cornelissen, Falster, Garnier, et al., 2005). We conducted the SMA regression analysis using the "smatr" package in R (version 4.2.1). Heterogeneity among SMA slopes was tested using a permutation test. A common slope was estimated when slope homogeneity was confirmed ($P > 0.05$). Elevation homogeneity was compared only when slopes were homogeneous. The original data were log-transformed (base 10), and subsequent SMA regressions were fitted to analyze relationships among leaf functional traits.

We utilized the global aridity index (AI) data sets (version 3) to represent the distribution of leaf traits across different climatic regions (Anderegg et al., 2021). Following the generalized UNEP climate classification scheme (UNEP, 1997), the global land surface was categorized into five areas based on AI values: hyper-arid ($AI < 0.03$), arid ($0.03 \le AI < 0.2$), semi-arid ($0.2 \le AI < 0.5$), dry sub-humid ($0.5 \le AI < 0.65$), and humid ($AI \ge 0.65$). The

21698961, 2026, 11, Downloaded from https://agupubs.onlinelibrary.wiley.com/doi/10.1029/2026JG010127 by Cornell University, Wiley Online Library on [06/11/2026]. See the Terms and Conditions (https://onlinelibrary.wiley.com/terms-and-conditions) on Wiley Online Library for rules of use; OA articles are governed by the applicable Creative Commons License

eCO_2 experiments used in this study encompassed all climate regions (Figure 2a). Specifically, humid areas accounted for the majority of the experimental sites (58.57%), followed by dry sub-humid (22.86%), semi-arid (10.00%), arid (4.29%), and hyper-arid (4.29%) regions.

2.2. CABLE Version 2 Land Surface Model

The Australian CABLE model (version 2) is a global land surface model designed to simulate carbon, water, and energy exchange processes between the land and atmosphere (Kowalczyk, 2006; Wang et al., 2010, 2011). The CABLE model fully couples the carbon, nitrogen, and phosphorus cycles to simulate biogeochemical processes (Wang et al., 2010, 2011). Through a series of simulation experiments, CABLE can be applied to explore nutrient limitations (Wei et al., 2022), attribution analysis (Zhang et al., 2016), uncertainty propagation (Bian & Xia, 2023), and plant feedback effects (Lei et al., 2019). The CABLE model has been extensively evaluated using a wide range of global observational data sets (Piao et al., 2015), eddy covariance flux measurements (Best et al., 2015), and manipulation field experiments (De Kauwe et al., 2014). These evaluations demonstrate that CABLE performs well and aligns closely with other process-based terrestrial ecosystem models.

The CABLE model includes nine organic nitrogen pools and one soil mineral nitrogen pool, based on the hypothesis that plants absorb only mineral nitrogen. The nitrogen cycle is modeled according to Wang et al. (2007), with changes in nitrogen pools represented by a set of differential equations. Plant nitrogen uptake is determined by a function of the size of the soil mineral N pool and the nitrogen demand for plant growth. Nitrogen demand is calculated as the product of the maximal nitrogen-to-carbon (N:C) ratio and the allocated net primary production, minus resorbed nitrogen. When nitrogen uptake exceeds demand, the absorbed nitrogen is allocated proportionally among the pools according to their respective demands. Conversely, when supply falls short of the minimal plant demand, nitrogen limitation occurs (Wang et al., 2010). In the default CABLE formulation, leaf nitrogen content depends not only on the N:C ratio but also on the balance between nitrogen uptake and demand, allowing it to vary within prescribed ranges (Table S2 in Supporting Information S1). Additionally, the CABLE model utilizes the IGBP biome classification (Figure S1 in Supporting Information S1).

In the CABLE model, GPP is calculated based on the LAI, the maximum Ribulose-1,5-bisphosphate (RuBP) carboxylase/oxygenase (Rubisco) carboxylation rate (v_{cmax}), and the maximum rate of electron transport for regeneration of RuBP (j_{max}) of the top canopy leaves at a standard leaf temperature of 25°C (Li et al., 2018; Wang et al., 2012). The LAI is calculated as

$$\mathrm{LAI} = \mathrm{C_{leaf}} \times \mathrm{SLA} \tag{7}$$

where C_{leaf} is the leaf carbon pool (gC m^{-2}), and SLA represents the specific leaf area. In the default model, SLA is assumed to be constant across plant functional types (Table S2 in Supporting Information S1). However, in our simulations, it is calibrated using response ratios derived from observational data sets (Equation 9). CABLE simulates C3 photosynthesis using the Farquhar et al. (1980) scheme and employs a Collatz-type extension of this scheme for C4 plants (Collatz et al., 1992), while using the same equation for v_{cmax} in both C3 and C4 plants. The term v_{cmax} is estimated as a linear function of leaf nitrogen content per unit leaf area (gN m^{-2}), expressed as

$$v_{\mathrm{cmax}} = a + b \times N_{\mathrm{a}} \tag{8}$$

The terms a and b are two empirical coefficients with values from Kattge et al. (2009) for each PFT (Table S3 in Supporting Information S1). For each model grid cell, the corresponding coefficients were assigned according to its PFT, while the trait-based N_a varied spatially because the grid-specific SLA was generated using Equation 9 and the corresponding N_a was subsequently estimated using Equation 10. Thus, the resulting v_{cmax} varied spatially among model grid cells. In the model, j_{max} is assumed to be twice v_{cmax} at a leaf temperature of 25°C (Leuning, 2002).

2.3. Incorporated Coordinated Trait Acclimation to the CABLE Model

In this study, the model was first spun up to a steady state in 1900 using the semi-analytical spin-up method from Xia et al. (2012). Subsequently, the CABLE model was run from 1901 to 1980 to generate a restart file for experiments starting in 1981. Finally, we conducted a series of experimental simulations, beginning in 1981, to

21698961, 2026, 11, Downloaded from https://agupubs.onlinelibrary.wiley.com/doi/10.1029/2026JG010127 by Cornell University, Wiley Online Library on [06/11/2026]. See the Terms and Conditions (https://onlinelibrary.wiley.com/terms-and-conditions) on Wiley Online Library for rules of use; OA articles are governed by the applicable Creative Commons License

test the coordinated trait acclimation effect on global photosynthesis under elevated CO_2. The CRUNCEP version 5 meteorological forcing data set was used to drive the CABLE simulations with a spatial resolution of 0.5° from 1901 to 2013. The annual mean global surface CO_2 concentration for 1901–2013 was reconstructed using a combination of Antarctic ice-core records and atmospheric observations (Keeling & Whorf, 2005). We conducted three sets of modeling simulations (Table S4 in Supporting Information S1) to examine the effects of different CO_2 and trait scenarios. The control simulation under ambient CO_2 (CK), driven by historical CO_2 levels with no changes to trait parameters, represents the baseline historical scenario. The eCO_2 simulation (EC), driven by time-varying CO_2 that doubles from 1981 to 2013 without altering trait parameters, represents the photosynthetic response to eCO_2 in the absence of coordinated trait acclimation. This idealized CO_2 doubling scenario enables comparison with eCO_2 experiments, in which CO_2 enrichment is typically significant and sustained. The acclimation simulation (Acc), driven by the same time-varying doubled CO_2 as the EC simulation, incorporates the coordinated trait acclimation relationship, thereby capturing their effects under eCO_2 conditions (Figure 1).

The effects of eCO_2 on SLA and N_a were tested using the Student's *t*-test and further incorporated into the model through parameterization. In this study, model parameters are calibrated using response ratios and coordinated trait relationships derived from experimental data using a meta-analysis. The effect of eCO_2 on SLA is integrated into the model and calculated as

$$SLA_e = SLA_a \times \left(1 + A_{\%SLA}\right) \tag{9}$$

where SLA_e and SLA_a represent the SLA under the eCO_2 and aCO_2 conditions, respectively, while $A_{\%SLA}$ represents the observed RR of SLA to eCO_2. $A_{\%SLA}$ is randomly sampled 200 times for each land pixel from a normal distribution derived from the observational data sets, and these samples were used to drive transient simulations and evaluate the robustness of the results (Table S4 in Supporting Information S1). Subsequently, N_a is estimated using the observed coordinated acclimation relationship under eCO_2 identified through SMA regression, and can be expressed by the following equation:

$$N_a = 151.36 \times SLA^{-0.93} \tag{10}$$

In the default CABLE carbon-nitrogen framework, leaf N is simulated prognostically. Its temporal variation reflects mineral N uptake and allocation to plant tissues, as well as N losses associated with leaf turnover, and the dynamically simulated leaf N status feeds back to v_{cmax} through the model's N-v_{cmax} coupling (Wang et al., 2007, 2010). In our acclimation simulations, after the restart state from the previous year was read, the trait-derived leaf N was used to replace the leaf N pool at the beginning of each annual simulation. During the subsequent simulation for each year, leaf N evolved prognostically through CABLE's coupled C-N cycle and was subsequently used to calculate v_{cmax}. Because the available observations were still limited at the individual PFT level to robustly estimate PFT-specific SLA-N_a relationships, the global relationship in Equation 10 was applied across PFTs as a generalized empirical constraint in the CABLE simulations.

2.4. Statistical Analysis

We evaluated photosynthetic sensitivity to eCO_2 using modeling results. The eCO_2 response ratios (e.g., R_{GPP}) were calculated for each key ecological or climate component (e.g., GPP, LAI, v_{cmax}, or AI) as the ratio of their values under eCO_2 to those under aCO_2, using the following equation:

$$R_X = X_e / X_a \tag{11}$$

where R_X represents the eCO_2 RR for any response variable X; X_e and X_a represent the simulated variable under eCO_2 and aCO_2, respectively. The coordinated acclimation effect (ΔR) is subsequently expressed as

$$\Delta R = R_{Acc} - R_{eCO_2} \tag{12}$$

where R_{Acc} and R_{eCO_2} represent the eCO_2 response ratios under coordinated acclimation (Acc) and elevated CO_2 (eCO_2) simulations, respectively. Additionally, the β-factor is calculated using the following equation:

21698961, 2026, 11, Downloaded from https://agupubs.onlinelibrary.wiley.com/doi/10.1029/2026JG010127 by Cornell University, Wiley Online Library on [06/11/2026]. See the Terms and Conditions (https://onlinelibrary.wiley.com/terms-and-conditions) on Wiley Online Library for rules of use; OA articles are governed by the applicable Creative Commons License

$$\beta = \log(X_e/X_a)/\log(e\mathrm{CO}_2/a\mathrm{CO}_2) \quad (13)$$

where β is a dimensionless parameter commonly used to quantify the apparent GPP response ratio to CO_2, facilitating comparisons with other studies (Chen et al., 2022; Walker et al., 2021).

To assess the impact of the magnitude and direction of key environmental drivers on R_{GPP}, we selected nine explanatory variables representing climate, vegetation structure, and physiological characteristics of high ecological importance. Previous studies (Hu et al., 2022; Madani et al., 2017, 2020; Yuan et al., 2019) have demonstrated that these factors significantly influence GPP and R_{GPP}. The variables include land surface air temperature (Tair), precipitation (prec), soil moisture (soilM), soil temperature (soilT), vapor pressure deficit (VPD), aridity index (AI), photosynthetically active radiation (PAR), leaf area index (LAI), and the maximum rate of Rubisco carboxylation (v_{cmax}). All explanatory variables were derived from the model's prognostic outputs rather than from climatological data sets to quantify coordinated acclimation within the model framework directly. Variables such as Tair, prec, soilM, soilT, VPD, and PAR remained consistent across all simulations, as the same set of meteorological forcings drove them. In contrast, LAI, v_{cmax}, and AI varied among simulations due to differences in CO_2 concentration, SLA, and N_a. Therefore, the eCO_2 response ratios for these variables were calculated using Equation 11 to quantify their effects on R_{GPP}. Furthermore, since VPD and AI were not directly available from the model output, VPD was calculated following the equation from Yuan et al. (2019). The AI, on the other hand, was calculated as the ratio of multi-year-averaged annual precipitation to annual potential evapotranspiration, quantifying precipitation availability relative to atmospheric water demand (Zomer et al., 2022).

We then employed a random forest model to quantify the relative importance of each of the nine variables, leveraging its ability to capture complex, non-linear relationships and interactions (Breiman, 2001). The model consisted of 100 decision trees, each trained on bootstrap samples from the data set, with a randomly selected subset of predictor variables at each split. The relative importance of each variable was determined by the mean decrease in accuracy, which measures the reduction in model performance when a variable is permuted across out-of-bag samples. The random forest model was implemented using the "scikit-learn" library in Python (Pedregosa et al., 2011), with a fixed random seed to ensure reproducibility.

3. Results

3.1. Coordinated Downregulation of Leaf Trait Relationship Under Elevated CO_2

We analyzed the changes in SLA and N_a under eCO_2 for each observation (Figure 2). Elevated CO_2 significantly reduced SLA by 14.7% and N_a by 6.5% (t-test; Figure S2 in Supporting Information S1). Notably, 86.8% of SLA observations and 67.8% of N_a observations exhibited a decreased RR, with the reduction in N_a being less pronounced than that in SLA. The response ratios of SLA and N_a to eCO_2 followed a normal distribution (Figure S2 in Supporting Information S1). SMA regression analysis further revealed that although the slope of the SLA ~ N_a relationship remained stable under eCO_2, its intercept significantly decreased (Figure 2d, Table S5 in Supporting Information S1). Further analyses across temperature groups showed a steeper slope at higher temperatures, accompanied by a consistent decrease in the intercept of the SLA ~ N_a relationship under eCO_2 across all temperature groups (Figure S3 and Table S5 in Supporting Information S1). This change in the relationship indicates a lower leaf N concentration for a given leaf area. Overall, the SLA-N_a relationship demonstrates a coordinated downregulation in response to elevated CO_2.

3.2. Reduced Simulated Sensitivity of Global Photosynthesis to Elevated CO_2

Modeling experiments revealed that elevated CO_2 significantly enhanced GPP during the simulation period from 1981 to 2013 (Figure 3). The estimated global annual GPP was 109.2 ± 8.7 Pg C yr^{-1} under CK simulations, which is closely aligned with satellite-derived estimates (110.5 ± 21.3 Pg C yr^{-1}; Yuan et al., 2010) and falls within the range of 83–172 Pg C yr^{-1} reported by other model-based studies (Jiang & Ryu, 2016; Jung et al., 2020; Lai et al., 2024). This consistency across both satellite-based and model-derived estimates supports the use of CABLE for examining the effects of coordinated trait acclimation on simulated photosynthetic sensitivity to elevated CO_2. Under EC simulations, the estimated GPP was 163.0 ± 5.5 Pg C yr^{-1}, while the Acc simulation yielded an estimated GPP of 151.3 ± 10.8 Pg C yr^{-1}. The EC simulation results revealed that the increase in GPP

21698961, 2026, 11, Downloaded from https://agupubs.onlinelibrary.wiley.com/doi/10.1029/2026JG010127 by Cornell University, Wiley Online Library on [06/11/2026]. See the Terms and Conditions (https://onlinelibrary.wiley.com/terms-and-conditions) on Wiley Online Library for rules of use; OA articles are governed by the applicable Creative Commons License

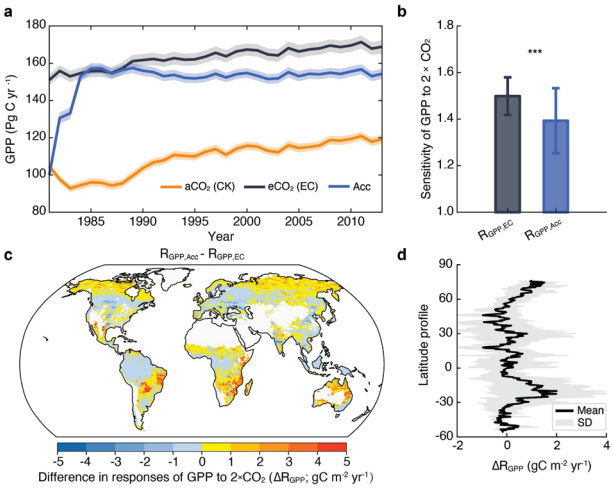


Figure 3. Simulated coordinated trait acclimation effect on the responses (elevated/ambient) of GPP to 2×CO_2. a, temporal dynamics of GPP in modeling experiment simulations from 1981 to 2013 under ambient CO_2 (CK, yellow), elevated CO_2 (EC, dark gray), and coordinated trait acclimation under elevated CO_2 (Acc, blue), with shaded areas representing the intra-annual variability. b, Means and the corresponding inter-annual variability (±S.D.) of the simulated responses from panel a, where "***" indicates that two simulated responses showed a significant difference at the level of $P < 0.001$ based on the *t*-test. c, The global pattern of the coordinated trait acclimation effect on the sensitivity of GPP to 2×CO_2. d, shows the corresponding latitude profile.

was smaller than the proportional increase in CO_2, suggesting that elevated CO_2 does not directly enhance GPP proportionally. Further analysis showed that the GPP response ratios (eCO_2:aCO_2) to doubled CO_2 were 1.50 ± 0.08 for EC and 1.39 ± 0.14 for Acc. Coordinated trait acclimation reduced the simulated GPP response to doubled CO_2 by 7.06%.

Spatially, compared to the CK simulation, eCO_2 increased simulated GPP globally (Figure S4 in Supporting Information S1), whereas Acc reduced GPP in specific regions, particularly in northern Europe and central North America (Figure S4 in Supporting Information S1). Coordinated trait acclimation enhanced the simulated GPP responses to doubled CO_2 in northern high latitudes, southeastern South America, southeastern Africa, and northern Australia (Figure 3c). Further analysis revealed that compared with EC, 40.7% of land pixels in the Acc simulation predicted substantially larger GPP increases, mainly located in dryland regions. In contrast, 33.0% of land pixels exhibited smaller increases, which were located primarily in humid forest regions, especially in the tropics, Europe, central North America, and Southeast Asia (Figure S5 in Supporting Information S1). The spatial pattern of the coordinated acclimation effect on GPP responses to doubled CO_2 (ΔR_{GPP}; Figure 3c) closely aligned with its impact on GPP (Acc-EC; Figure S5 in Supporting Information S1). These findings indicate that reduced GPP responses (ΔR_{GPP}) occurred primarily in humid forest regions, driven by coordinated trait acclimation. Analysis of the latitude profile revealed that coordinated trait acclimation led to larger simulated responses in mid- and high-latitude regions, while smaller responses occurred in the tropical areas (Figure 3d).

21698961, 2026, 11, Downloaded from https://agupubs.onlinelibrary.wiley.com/doi/10.1029/2026JG010127 by Cornell University, Wiley Online Library on [06/11/2026]. See the Terms and Conditions (https://onlinelibrary.wiley.com/terms-and-conditions) on Wiley Online Library for rules of use; OA articles are governed by the applicable Creative Commons License

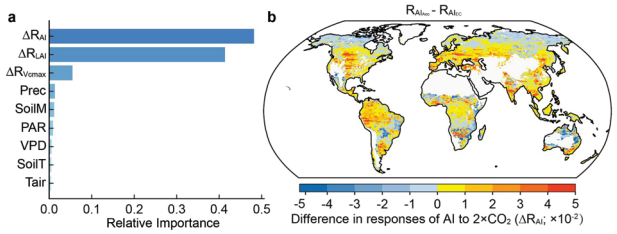


Figure 4. Dominant factors of the coordinated trait effect on GPP. a, The relative importance of the influencing factors based on the random forest models according to the global land pixels. b, The global pattern of the dominant factor (Aridity Index, AI) in coordinated trait acclimation effect on the sensitivity of GPP to 2×CO_2.

These results highlight the significant spatial heterogeneity of simulated global photosynthesis sensitivity to elevated CO_2 under coordinated trait acclimation.

3.3. Aridity Change as a Major Driver of Global GPP Response to Coordinated Trait Acclimation

Using a random forest model, we further identified the primary drivers most closely associated with the spatial pattern of the simulated coordinated trait effect on GPP (ΔR_{GPP}) at the global land scale. The results indicated that the variation in the coordinated acclimation effect on aridity responses to doubled CO_2 (ΔR_{AI}) accounted for 48.2% of the spatial variance in ΔR_{GPP}, followed by the coordinated trait effect on LAI (ΔR_{LAI}; 41.4%) and on v_{cmax} (ΔR_{vcmax}; 5.5%) (Figure 4a). Moreover, ΔR_{AI} exhibited a spatial pattern that contrasts with that of ΔR_{GPP} (Figures 3c and 4b). Specifically, the negative effect of coordinated trait acclimation mostly occurs in northern high-latitude and extratropical regions. In contrast, positive effects are primarily observed in evergreen broadleaf forest and grassland regions (Figure 4b). Further analysis revealed that changes in AI were driven mainly by variations in potential evapotranspiration and soil environments (Figure S6 in Supporting Information S1), which were influenced by LAI under acclimation to CO_2 (Figure S7 in Supporting Information S1). These findings indicate that ΔR_{GPP} is strongly associated with the aridity change (Figure 5a). Observational data sets provide further evidence supporting the links between aridity and trait relationships (Figure S8 and Table S6 in Supporting Information S1). Consistent with global spatial patterns, ΔR_{AI}, ΔR_{LAI}, and ΔR_{vcmax} appear to be the main contributors across climate zones. In contrast, other climate variables (i.e., Tair, VPD, Prec, SoilT, and soilM) contribute relatively little (Figures 5b–5f). Notably, in the hyper-arid region, ΔR_{LAI} accounted for 23.3% of the variance in ΔR_{GPP}, while air temperature (Tair), VPD, and ΔR_{AI} contributed 17.3%, 16.3%, and 11.2%, respectively. However, as this region represents only a small portion of the global vegetated land area, its overall contribution to global ΔR_{GPP} is minimal (Figure 5b).

4. Discussions

4.1. Downregulation of SLA-N_a Correlation Under eCO_2

Immobile plants acclimate to rapidly changing environments by altering their structural and functional traits to maximize their carbon gain. This study explored the responses of SLA and N_a to eCO_2 by analyzing data sets compiled from a series of eCO_2 experiments. The results revealed that eCO_2 generally reduces both SLA and N_a, although their responses exhibit substantial variability across species (Figures S2 and S9 in Supporting Information S1). The reduction in N_a and SLA under eCO_2 aligns well with previous experimental evidence (Poorter et al., 2022; Figure S10 in Supporting Information S1), providing further support for our results. The substantial variability underscores the high plasticity of leaf traits in response to rising CO_2 concentrations. Further analysis revealed that ignoring species variability inevitably introduces additional uncertainty into the CABLE-based simulations, leading to changes in GPP ranging from 0.01 to 0.24 Pg C yr^{-1} (Figure S11 in Supporting Information S1).

21698961, 2026, 11, Downloaded from https://agupubs.onlinelibrary.wiley.com/doi/10.1029/2026JG010127 by Cornell University, Wiley Online Library on [06/11/2026]. See the Terms and Conditions (https://onlinelibrary.wiley.com/terms-and-conditions) on Wiley Online Library for rules of use; OA articles are governed by the applicable Creative Commons License

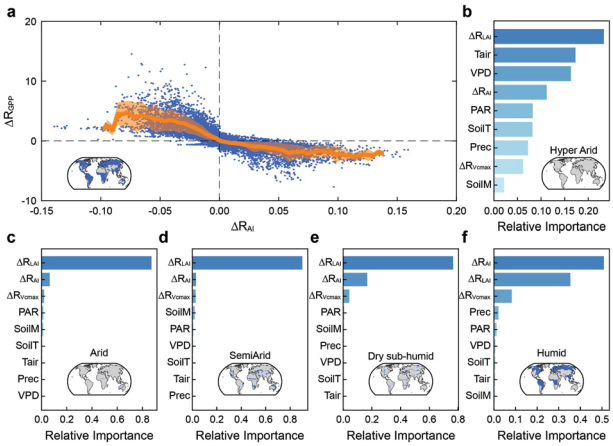


Figure 5. Global distribution of the coordinated trait effect on GPP and on aridity index. a, The spatial pattern of the coordinated trait effect on GPP (ΔR_{GPP}) along with the effect on aridity gradient (ΔR_{AI}). Each land pixel is represented by a blue point. Yellow scatter shows the grouped mean value of ΔR_{GPP} along with ΔR_{AI} gradient, grouped in 4×10^{-3}. The grouped standard deviation is represented by the shading areas. b–f, Relative importance of the factors in each climate region.

We found robust downregulation under eCO_2, manifested as a lower intercept in the log-log relationship between SLA and N_a at both the global scale and across climatic zones (Figure 2d, Figures S3 and S8 in Supporting Information S1). A previous study has indicated that although photosynthetic and economic leaf traits may decouple with increasing CO_2 concentrations (Blackman et al., 2016), the coordination between leaf traits remains unchanged (Figures 2d and Blackman et al., 2016; Cui et al., 2020). Further analysis based on mass-based leaf nitrogen content revealed stronger correlations among leaf traits compared to those based on area-based nitrogen (Wright et al., 2004; Figure S12 in Supporting Information S1), although the reductions in elevation were smaller than those in the area-based results (Table S7 in Supporting Information S1). This robust leaf trait relationship indicates that plants retain their inherent acquisitive-conservative growth strategy under elevated CO_2. Although the magnitude and direction of SLA and N_a responses to eCO_2 vary across species (Figure S9 in Supporting Information S1), eCO_2 does not alter their coordination pattern. Instead, it causes a parallel decrease in the intercept of the SLA $\sim N_a$ scaling relationship, reflecting a proportional reduction in the log-log relationship of both traits (Figure 2d, Figure S9 in Supporting Information S1). Our results also showed that leaf traits across different species can form new trait combinations adapted to eCO_2 (Figure S9 in Supporting Information S1), and these combinations continue to align along a single axis of variation, consistent with a unified leaf economic spectrum (Reich, 2014; Reich et al., 1997; Wright, Reich, Cornelissen, Falster, Garnier, et al., 2005). Moreover, we found that current coordination relationships are derived mainly from C3 plants, as eCO_2 has no significant effect on either SLA or N_a in C4 plants due to limited C4 data sets (Figure S13 in Supporting Information S1). Further analysis indicated that SLA responses to eCO_2 differed significantly between C3 and C4 plants, with 11.4% decreases in C3 plants and 3.5% increases in C4 plants (Figure S13 in Supporting Information S1). These results suggest that the responses of C4 plants to elevated CO_2 remain uncertain and require further validation with additional data sets in future studies.

21698961, 2026, 11, Downloaded from https://agupubs.onlinelibrary.wiley.com/doi/10.1029/2026JG010127 by Cornell University, Wiley Online Library on [06/11/2026]. See the Terms and Conditions (https://onlinelibrary.wiley.com/terms-and-conditions) on Wiley Online Library for rules of use; OA articles are governed by the applicable Creative Commons License

21698961, 2026, 11, Downloaded from https://agupubs.onlinelibrary.wiley.com/doi/10.1029/2026JG010127 by Cornell University, Wiley Online Library on [06/11/2026]. See the Terms and Conditions (https://onlinelibrary.wiley.com/terms-and-conditions) on Wiley Online Library for rules of use; OA articles are governed by the applicable Creative Commons License

An increased sensitivity of N_a to SLA was further observed across the temperature gradient (Figure S3 and Table S5 in Supporting Information S1), indicating that plants in high-temperature regions may invest more N in leaf construction to support their physiological functions. Recent isotope evidence based on $\delta^{15}N$ has demonstrated a linear increase in plant N use with rising mean annual temperature (Hu et al., 2024; Wang, 2024). Additionally, the SLA $\sim N_a$ relationship also varied across aridity groups (Figure S8 and Table S6 in Supporting Information S1), indicating environmental modulation of this relationship. Nevertheless, the elevation shifted downward under elevated CO_2 across all temperature and aridity groups, with broadly similar magnitudes of shift. These results suggest that the eCO_2-induced downward shift in the SLA $\sim N_a$ relationship is broadly consistent across climatic conditions despite some environmental heterogeneity. Given the limited observations available for individual PFTs, incorporating a relationship estimated from the global data set inevitably introduces additional uncertainty and may bias N_a estimates across both temperature and aridity gradients (Figures S3, S8, Tables S5, and S6 in Supporting Information S1). Therefore, the SLA $\sim N_a$ relationship used in this study focuses on the empirically observed coordinated acclimation of SLA and N_a under elevated CO_2, rather than dynamically representing trait responses to all changing environmental drivers. Declining N availability has been widely reported across terrestrial ecosystems (Mason et al., 2022), and recent tree-ring $\delta^{15}N$ evidence suggests that rising atmospheric CO_2 may further reduce N availability in boreal forests (Bassett et al., 2026). Other studies based on photosynthetic optimality theory have found that the reduction in leaf N content with eCO_2 is primarily driven by a decreased demand for leaf N (Bassiouni et al., 2025; Dong et al., 2022; Smith & Keenan, 2020; Stocker et al., 2025). This reduction may allow the surplus N to be allocated to other tissues, potentially enhancing their growth and mitigating N limitations on plant growth (Smith et al., 2024). Although the model used in this study does not incorporate this theoretical relationship, integrating experimentally derived findings into land surface models could offer new insights into the plant-mediated global carbon-concentration feedback, especially since most land surface models simulate photosynthesis as a function of leaf N.

4.2. Coordinated Trait Acclimation Reduced Simulated Photosynthesis Sensitivity to eCO_2

Compared to the EC simulation, the globally averaged GPP increases rapidly in the first few years but declines slightly when coordinated trait acclimation is incorporated (Figure 3a). The initial increase in GPP closely tracked the rapid increase in LAI, while GPP per unit LAI changed only slightly, indicating that the early GPP response was mainly associated with canopy development rather than a strong increase in photosynthetic productivity per unit leaf area. As LAI approached a stable level, GPP also leveled off and subsequently declined slightly. Coordinated trait acclimation reduced the simulated GPP response to doubled CO_2 (Figure 3b). This reduction was primarily observed in forest regions, especially in tropical evergreen broadleaf forests, Europe, eastern Asia, the central plains of North America, and southern Europe (Figure 3c). The reduction was mainly driven by the negative effect of coordinated leaf trait acclimation on LAI rather than the positive effect on v_{cmax} (Figure S7 in Supporting Information S1). In contrast, in mid- and high-latitude regions of North America and northern Europe, the reduction was primarily associated with the negative effect on v_{cmax} (Figure S7 in Supporting Information S1). The positive coordinated acclimation effect on v_{cmax} arises mainly because the control simulation under aCO_2 used the PFT-specific SLA prescribed by the model and did not incorporate the coordinated trait relationship. Further analysis based on the observed SLA $\sim N_a$ relationship and Equation 8 showed reductions in leaf nitrogen content and v_{cmax} under eCO_2 (Text S1 in Supporting Information S1), which are highly consistent with previous experimental evidence (Ainsworth & Long, 2005; Leakey et al., 2009; Poorter et al., 2022), supporting our CABLE-based simulation results. In the current CABLE formulation, j_{max} is prescribed as twice v_{cmax}, so coordinated acclimation-induced reductions in N_a decrease both v_{cmax} and j_{max} proportionally. A shift between Rubisco- and RuBP-regeneration-limited photosynthesis may modulate the realized response under eCO_2 (Haverd et al., 2020), but its relative contribution could not be further quantified from the existing model outputs.

Coordinated trait acclimation reduced simulated GPP responses to doubled CO_2, but the magnitude of this reduction varied substantially across space. In particular, regions where the results are constrained by the model's default maximum LAI and C:N ratio limits may introduce uncertainties and lead to some unnatural patterns (Figures S7 and S14 in Supporting Information S1). By further isolating the effects of coordination (aCO_2 + Coordination-only) and acclimation (eCO_2 + Acclimation-only) on GPP (Table S4 in Supporting Information S1), we found that the estimated global GPP was 72.9 ± 5.3 Pg C yr^{-1} for coordination and 166.3 ± 15.7 Pg C yr^{-1} for acclimation. Further analysis showed that the GPP response ratios (eCO_2:aCO_2) were

21698961, 2026, 11, Downloaded from https://agupubs.onlinelibrary.wiley.com/doi/10.1029/2026JG010127 by Cornell University, Wiley Online Library on [06/11/2026]. See the Terms and Conditions (https://onlinelibrary.wiley.com/terms-and-conditions) on Wiley Online Library for rules of use; OA articles are governed by the applicable Creative Commons License

0.67 ± 0.06 and 1.53 ± 0.15 for coordination and acclimation, respectively (Figure S15 in Supporting Information S1). These results demonstrate that incorporating coordinated leaf trait relationships substantially reduces simulated GPP, whereas acclimation alone enhances ecosystem carbon input relative to the eCO_2 simulation. Consequently, jointly accounting for both coordination and acclimation is essential for producing robust and credible estimates of simulated GPP responses to rising CO_2. In addition, we note that the global annual GPP under ambient CO_2 is slightly lower than estimates from observationally based data sets (Lai et al., 2024; Welp et al., 2011) and other land surface models (Jung et al., 2020), mainly reflecting the influence of the coupled phosphorus cycle in CABLE. Given that our conclusions are based on relative GPP responses to rising CO_2, which are less sensitive to baseline magnitude, the slightly lower GPP has limited implications for our results.

Two additional analyses thoroughly examined the reduced simulated GPP responses to elevated CO_2 levels resulting from coordinated trait acclimation. First, two commonly used approaches (Keenan et al., 2023; Piao et al., 2013) were employed to estimate the sensitivity of global photosynthesis to elevated CO_2 (β_{GPP}). The results from both methods consistently showed a reduction in simulated β_{GPP} when coordinated trait acclimation was incorporated (Text S2 in Supporting Information S1). The spatial results also reveal a similar pattern: tropical forests dominated the reduction in β_{GPP} (Text S2 in Supporting Information S1). Second, a further sensitivity analysis of the Acc simulations, derived from randomly selected $RR_{\%SLA}$ (Methods), showed that the reduced simulated GPP responses to doubled CO_2 were not sensitive to the chosen parameters (Figure S16 in Supporting Information S1). The largest uncertainty was observed in forest regions (Figure S14 in Supporting Information S1), highlighting potential systematic uncertainties in terrestrial ecosystem models regarding how photosynthesis responds to elevated CO_2. These errors can be attributed to several widely reported reasons, such as the general representation of v_{cmax} as a fixed constant or a linear function of leaf nitrogen content (Ali et al., 2015), insufficient representation of disturbance from both natural (Lloret et al., 2012; Walker et al., 2019) and human activities (Achat et al., 2015; Fawcett et al., 2023), and the potential effects of woody shrub expansion (Stevens et al., 2017).

Given that the changes in GPP in our simulations include both direct CO_2 and non-CO_2 effects, the CO_2 responses explored in this study reflect the combined effects of these two factors. A further logarithmic transformation following Walker et al. (2021) has been performed to facilitate comparison with other studies. The reduction in photosynthetic sensitivity to elevated CO_2 (β_{GPP}) was then quantified by incorporating the coordinated trait acclimation relationship into the model (Figure S17 in Supporting Information S1). The multi-year averaged β_{GPP} is 0.58 ± 0.08 under EC and 0.48 ± 0.14 under Acc. Both are relatively lower than those reported in other observation-based studies (Figure S17 in Supporting Information S1). For example, Keenan et al. (2023) constrained the increase in GPP under rising CO_2 by integrating global models with remote sensing data, estimating a β_{GPP} of 0.62 ± 0.14. This result is lower than the estimate from the satellite-based evapotranspiration and analytical ecosystem water-use efficiency model, which reported a β_{GPP} of 1.1 ± 0.5 (Cheng et al., 2017). Other studies based on deuterium isotopomers (Ehlers et al., 2015), eddy-covariance (Fernández-Martínez et al., 2017), and ice-core measurements of carbonyl sulfide (Campbell et al., 2017) have reported relatively high β_{GPP}, estimates as 1.0, 1.2 ± 0.6, and 0.95 ± 0.2, respectively. Although our results are lower than those from other observational data sets, they still fall within the range of 0.12–0.9 reported by other modeling studies (Figure S17 in Supporting Information S1; Chen et al., 2022), supporting the recently proposed weak land sink hypothesis (Randerson et al., 2025). At the site level, CABLE overestimated absolute GPP at both EucFACE (Yang et al., 2020) and Duke FACE (Schäfer et al., 2003), particularly at EucFACE (Figure S18 in Supporting Information S1). This overestimation was evident under both ambient and elevated CO_2 conditions, whereas the simulated β_{GPP} remained broadly comparable to the FACE-derived estimates. At EucFACE, coordinated trait acclimation reduced β_{GPP} in the same direction as the reduction associated with observed v_{cmax} acclimation reported by Yang et al. (2020). Differences in measurement approaches, spatial-temporal resolution, and study periods inevitably introduce uncertainty into these comparisons. Overall, these findings underscore the limited understanding of photosynthetic responses to rising CO_2 in terrestrial ecosystem models.

The reduced GPP responses to elevated CO_2 simulated in our study contrast with the higher CO_2 fertilization reported by Haverd et al. (2020), likely reflecting differences in the coordination processes represented. At the leaf level, reduced photosynthetic N investment tends to lower v_{cmax} and weaken the CO_2 response (Bassiouni et al., 2025), whereas Haverd et al. (2020) dynamically optimized j_{max}/v_{cmax} to coordinate carboxylation and electron transport and thereby maintain more efficient photosynthetic coordination. In contrast, our simulations represent CO_2-driven acclimation of SLA, which affects leaf-to-canopy structural scaling, but do not dynamically

optimize j_{max}/v_{cmax}. These processes are not mutually exclusive and may have counteracting effects on simulated CO_2 fertilization. Thus, GPP responses to elevated CO_2 likely depend on the combined responses of photosynthetic N investment, its allocation between carboxylation and electron transport, and leaf-to-canopy structural scaling.

4.3. Aridity Change Dominates Spatial Variation in Photosynthetic Sensitivity to eCO_2

We analyzed the contributions of environmental factors, leaf structure, and physiological traits to the spatial variability in simulated photosynthetic response to rising CO_2. Our findings indicate that aridity change accounted for the largest variation in simulated photosynthetic sensitivity to elevated CO_2 (48.2%), followed by LAI (41.4%) and maximum photosynthetic rate (5.5%) (Figures 4a and 5). A growing body of evidence from other studies demonstrates that water availability significantly regulates leaf traits (Figure S8 in Supporting Information S1), thereby influencing photosynthetic sensitivity to eCO_2. For instance, previous studies on hydraulic traits have demonstrated that leaf thickness (related to SLA) and leaf nitrogen content are closely associated with water availability (Nardini et al., 2012; Rosas et al., 2019). Specifically, plants in humid regions typically exhibit leaf traits aligned with a "fast" growth strategy for resource acquisition (Rosas et al., 2019). In contrast, plants in arid regions, characterized by high leaf nitrogen concentrations, tend to adopt a resource-conservative ("slow") strategy to enhance tolerance to water stress (Rosas et al., 2019; Wright, Reich, Cornelissen, Falster, Groom, et al., 2005; Wright & Westoby, 2002). A recent study based on trait data sets further demonstrates that plants generally incur higher water costs than nutrient costs (Westerband et al., 2023), underscoring the critical role of water availability in shaping trait relationships (Wright, Reich, Cornelissen, Falster, Groom, et al., 2005).

In addition, elevated CO_2 can increase leaf-level water use efficiency (WUE) by allowing plants to maintain carbon assimilation with lower stomatal conductance, thereby reducing water loss per unit carbon gain. In the CABLE model, WUE responses are represented through the coupled photosynthesis-stomatal conductance scheme using the Ball-Berry-Leuning (Leuning et al., 1995) model. At the same time, a high VPD and limited soil water availability can still restrict stomatal opening, constrain CO_2 diffusion into leaves, and limit photosynthesis, particularly in arid and semi-arid regions. Therefore, the strong contribution of aridity changes identified here should be interpreted with caution, as it may reflect integrated hydroclimatic constraints involving water availability, atmospheric water demand, stomatal regulation, and WUE.

Coordinated trait acclimation influences photosynthetic sensitivity to eCO_2 in two key ways. First, increased leaf thickness and reduced leaf nitrogen content directly enhance the net photosynthetic rate under eCO_2 (Poorter et al., 2022). Second, changes in vegetation canopy structure driven by SLA can influence biophysical processes, such as evapotranspiration and atmospheric circulation (Tietjen et al., 2017; Yang et al., 2019; Zeng et al., 2017), which in turn affect the local climate. Specifically, the accumulation of nonstructural carbohydrates in leaves, driven by coordinated acclimation (Luo et al., 1994; Poorter et al., 1997, 2009), enhanced leaf thickness and thereby reduced evapotranspiration and LAI in humid regions (Kovenock & Swann, 2018). In addition, coordinated trait acclimation under eCO_2 reduced stomatal conductance (Ainsworth & Rogers, 2007) and enhanced drought resistance by increasing leaf-level water-use efficiency (Pastore et al., 2019). In arid regions, the influence of water availability on stomatal conductance can outweigh that of CO_2 (Ainsworth & Rogers, 2007; Leakey et al., 2009). Consequently, the simulated sensitivity of photosynthesis to elevated CO_2 in arid regions is more vulnerable to changes in vegetation structure (Figures 5b–5e), which in turn impacts potential evapotranspiration and soil environments by biophysical feedback (Cui et al., 2022; Piao et al., 2020). Other eddy-flux observations have shown the decoupling of LAI and GPP along aridity gradients (Hu et al., 2022), demonstrating the key regulatory role of aridity in photosynthetic productivity.

5. Conclusion

Trait-based relationships are a promising approach for improving model simulations and predictions. Although considerable research has explored how plant traits respond to rising CO_2, few studies have investigated the influence of coordinated trait relationships on simulated photosynthesis sensitivity to elevated CO_2. This study reveals a consistent decrease in the intercept of the log-log relationship between leaf structural and physiological traits under elevated CO_2. By integrating this relationship into the CABLE model, we found that coordinated trait acclimation reduces simulated photosynthetic sensitivity to elevated CO_2, with its spatial variation primarily driven by changes in aridity gradients. These findings suggest that current dynamic global vegetation models may

21698961, 2026, 1, Downloaded from https://agupubs.onlinelibrary.wiley.com/doi/10.1029/2026JG010127 by Cornell University, Wiley Online Library on [06/11/2026]. See the Terms and Conditions (https://onlinelibrary.wiley.com/terms-and-conditions) on Wiley Online Library for rules of use; OA articles are governed by the applicable Creative Commons License

overestimate photosynthetic responses to CO_2, potentially leading to an overly optimistic assessment of terrestrial ecosystems' capacity to mitigate rising CO_2 levels. However, the magnitude of this overestimation remains uncertain, as it is difficult to quantify the contributions of increased leaf-level water- and nitrogen-use efficiency, which can enhance ecosystem carbon uptake and partly offset the bias (Smith et al., 2024). Furthermore, our results underscore the critical role of aridity changes in regulating simulated photosynthetic responses to rising CO_2. This study bridges the gap between leaf trait responses to CO_2 and ecosystem-level carbon-concentration feedback.

Conflict of Interest

The authors declare no conflicts of interest relevant to this study.

Availability Statement

Documentation describing how to install, compile, and run the CABLE model is available at https://cable.readthedocs.io/en/latest/user_guide/. The CABLE source code used to conduct all simulations in this study is available on GitHub at https://github.com/cyBian/CABLE_Trait_Acclimation, and on Figshare at https://doi.org/10.6084/m9.figshare.32415735.v1 (Bian, 2026a). The CRUNCEP atmospheric forcing data sets are available at https://gdex.ucar.edu/datasets/d314003/ (Viovy, 2018). The key model output variables, processing scripts, and associated metadata files are available at https://doi.org/10.6084/m9.figshare.32417247.v2 (Bian, 2026b). The aridity index data set is available at https://doi.org/10.6084/m9.figshare.7504448.v5 (Trabucco & Zomer, 2019).

Acknowledgments
This work was financially supported by the National Key R&D Program of China (2022YFF0802104), the National Natural Science Foundation of China (32325033), the Fundamental and Interdisciplinary Disciplines Breakthrough Plan of the Ministry of Education of China (JYB2025XDXM904), and the Shanghai Pilot Program for Basic Research (TQ20220102). We thank Nicholas Smith for his constructive suggestions, which helped us improve the manuscript. We thank two anonymous reviewers for their helpful and constructive comments on the manuscript.

References

Achat, D., Fortin, M., Landmann, G., Ringeval, B., & Augusto, L. (2015). Forest soil carbon is threatened by intensive biomass harvesting. *Scientific Reports*, *5*(1), 15991. https://doi.org/10.1038/srep15991

Ainsworth, E. A., & Long, S. P. (2005). What have we learned from 15 years of free-air CO_2 enrichment (FACE)? A meta-analytic review of the responses of photosynthesis, canopy properties and plant production to rising CO_2. *New Phytologist*, *165*(2), 351–372. https://doi.org/10.1111/j.1469-8137.2004.01224.x

Ainsworth, E. A., & Rogers, A. (2007). The response of photosynthesis and stomatal conductance to rising [CO_2]: Mechanisms and environmental interactions. *Plant, Cell & Environment*, *30*(3), 258–270. https://doi.org/10.1111/j.1365-3040.2007.01641.x

Ali, A. A., Xu, C., Rogers, A., McDowell, N. G., Medlyn, B. E., Fisher, R. A., et al. (2015). Global-scale environmental control of plant photosynthetic capacity. *Ecological Applications*, *25*(8), 2349–2365. https://doi.org/10.1890/14-2111.1

Anderegg, L. D. L., Loy, X., Markham, I. P., Elmer, C. M., Hovenden, M. J., HilleRisLambers, J., & Mayfield, M. M. (2021). Aridity drives coordinated trait shifts but not decreased trait variance across the geographic range of eight Australian trees. *New Phytologist*, *229*(3), 1375–1387. https://doi.org/10.1111/nph.16795

Bassett, K. R., Hupperts, S. F., Jämtgård, S., Oxlund, L., Fridman, J., Perakis, S. S., & Gundale, M. J. (2026). Rising atmospheric CO2 reduces nitrogen availability in boreal forests. *Nature*, *650*(8102), 629–635. https://doi.org/10.1038/s41586-025-10039-5

Bassiouni, M., Smith, N. G., Reu, J. C., Peñuelas, J., & Keenan, T. F. (2025). Observed declines in leaf nitrogen explained by photosynthetic acclimation to CO_2. *Proceedings of the National Academy of Sciences*, *122*(33), e2501958122. https://doi.org/10.1073/pnas.2501958122

Best, M. J., Abramowitz, G., Johnson, H. R., Pitman, A. J., Balsamo, G., Boone, A., et al. (2015). The plumbing of land surface models: Benchmarking model performance. *Journal of Hydrometeorology*, *16*(3), 1425–1442. https://doi.org/10.1175/JHM-D-14-0158.1

Bian, C. (2026a). CABLE: Coordinated leaf trait acclimation reduces simulated global photosynthesis sensitivity to elevated CO_2 in a land surface model. (Version 2) [Software]. *Figshare*. https://doi.org/10.6084/m9.figshare.32415735.v1

Bian, C. (2026b). Data, model output, processing and analysis code used in "coordinated leaf trait acclimation reduces simulated global photosynthesis sensitivity to elevated CO_2 in a land surface model" (Version 2). [Dataset]. *Figshare*. https://doi.org/10.6084/m9.figshare.32417247.v2

Bian, C., & Xia, J. (2023). Uncertainty propagation in a global biogeochemical model driven by leaf area data. *Frontiers in Ecology and Evolution*, *11*, 1105832. https://doi.org/10.3389/fevo.2023.1105832

Blackman, C. J., Aspinwall, M. J., Resco de Dios, V., Smith, R. A., & Tissue, D. T. (2016). Leaf photosynthetic, economics and hydraulic traits are decoupled among genotypes of a widespread species of eucalypt grown under ambient and elevated CO_2. *Functional Ecology*, *30*(12), 1491–1500. https://doi.org/10.1111/1365-2435.12666

Breiman, L. (2001). Random forests. *Machine Learning*, *45*(1), 5–32. https://doi.org/10.1023/A:1010933404324

Campbell, J. E., Berry, J. A., Seibt, U., Smith, S. J., Montzka, S. A., Launois, T., et al. (2017). Large historical growth in global terrestrial gross primary production. *Nature*, *544*(7648), 84–87. https://doi.org/10.1038/nature22030

Chen, C., Riley, W. J., Prentice, I. C., & Keenan, T. F. (2022). CO_2 fertilization of terrestrial photosynthesis inferred from site to global scales. *Proceedings of the National Academy of Sciences*, *119*(10), e2115627119. https://doi.org/10.1073/pnas.2115627119

Cheng, L., Zhang, L., Wang, Y. P., Canadell, J. G., Chiew, F. H. S., Beringer, J., et al. (2017). Recent increases in terrestrial carbon uptake at little cost to the water cycle. *Nature Communications*, *8*(1), 110. https://doi.org/10.1038/s41467-017-00114-5

Collatz, G. J., Ribas-Carbo, M., & Berry, J. A. (1992). Coupled photosynthesis-stomatal conductance model for leaves of C4 plants. *Functional Plant Biology*, *19*(5), 519–538. https://doi.org/10.1071/pp9920519

Cui, E., Weng, E., Yan, E., & Xia, J. (2020). Robust leaf trait relationships across species under global environmental changes. *Nature Communications*, *11*(1), 2999. https://doi.org/10.1038/s41467-020-16839-9

Cui, E., Xia, J., & Luo, Y. (2023). Nitrogen use strategy drives interspecific differences in plant photosynthetic CO_2 acclimation. *Global Change Biology*, *29*(13), 3667–3677. https://doi.org/10.1111/gcb.16706

21698961, 2026, 11, Downloaded from https://agupubs.onlinelibrary.wiley.com/doi/10.1029/2026JG010127 by Cornell University, Wiley Online Library on [06/11/2026]. See the Terms and Conditions (https://onlinelibrary.wiley.com/terms-and-conditions) on Wiley Online Library for rules of use; OA articles are governed by the applicable Creative Commons License

Cui, J., Lian, X., Huntingford, C., Gimeno, L., Wang, T., Ding, J., et al. (2022). Global water availability boosted by vegetation-driven changes in atmospheric moisture transport. *Nature Geoscience*, *15*(12), 982–988. https://doi.org/10.1038/s41561-022-01061-7

Davies-Barnard, T., Meyerholt, J., Zaehle, S., Friedlingstein, P., Brovkin, V., Fan, Y., et al. (2020). Nitrogen cycling in CMIP6 land surface models: Progress and limitations. *Biogeosciences*, *17*(20), 5129–5148. https://doi.org/10.5194/bg-17-5129-2020

De Kauwe, M. G., Medlyn, B. E., Zaehle, S., Walker, A. P., Dietze, M. C., Wang, Y. P., et al. (2014). Where does the carbon go? A model-data intercomparison of vegetation carbon allocation and turnover processes at two temperate forest free-air CO_2 enrichment sites. *New Phytologist*, *203*(3), 883–899. https://doi.org/10.1111/nph.12847

Dong, N., Prentice, I. C., Evans, B. J., Caddy-Retalic, S., Lowe, A. J., & Wright, I. J. (2017). Leaf nitrogen from first principles: Field evidence for adaptive variation with climate. *Biogeosciences*, *14*(2), 481–495. https://doi.org/10.5194/bg-14-481-2017

Dong, N., Wright, I. J., Chen, J., Luo, X., Wang, H., Keenan, T. F., et al. (2022). Rising CO_2 and warming reduce global canopy demand for nitrogen. *New Phytologist*, *235*(5), 1692–1700. https://doi.org/10.1111/nph.18076

Ehlers, I., Augusti, A., Betson, T. R., Nilsson, M. B., Marshall, J. D., & Schleucher, J. (2015). Detecting long-term metabolic shifts using isotopomers: CO_2-driven suppression of photorespiration in C3 plants over the 20th century. *Proceedings of the National Academy of Sciences*, *112*(51), 15585–15590. https://doi.org/10.1073/pnas.1504493112

Evans, J. R. (1989). Photosynthesis and nitrogen relationships in leaves of C3 plants. *Oecologia*, *78*(1), 9–19. https://doi.org/10.1007/BF00377192

Farquhar, G. D., von Caemmerer, S., & Berry, J. A. (1980). A biochemical model of photosynthetic CO_2 assimilation in leaves of C3 species. *Planta*, *149*(1), 78–90. https://doi.org/10.1007/BF00386231

Fawcett, D., Sitch, S., Ciais, P., Wigneron, J. P., Silva-Junior, C. H. L., Heinrich, V., et al. (2023). Declining amazon biomass due to deforestation and subsequent degradation losses exceeding gains. *Global Change Biology*, *29*(4), 1106–1118. https://doi.org/10.1111/gcb.16513

Fernández-Martínez, M., Vicca, S., Janssens, I. A., Ciais, P., Obersteiner, M., Bartrons, M., et al. (2017). Atmospheric deposition, CO_2, and change in the land carbon sink. *Scientific Reports*, *7*(1), 9632. https://doi.org/10.1038/s41598-017-08755-8

Friedlingstein, P., Meinshausen, M., Arora, V. K., Jones, C. D., Anav, A., Liddicoat, S. K., & Knutti, R. (2014). Uncertainties in CMIP5 climate projections due to carbon cycle feedbacks. *Journal of Climate*, *27*(2), 511–526. https://doi.org/10.1175/JCLI-D-12-00579.1

Harper, A. B., Cox, P. M., Friedlingstein, P., Wiltshire, A. J., Jones, C. D., Sitch, S., et al. (2016). Improved representation of plant functional types and physiology in the joint UK land environment simulator (JULES v4.2) using plant trait information. *Geoscientific Model Development*, *9*(7), 2415–2440. https://doi.org/10.5194/gmd-9-2415-2016

Haverd, V., Smith, B., Nieradzik, L. P., Briggs, P. R., Woodgate, W., Trudinger, C. M., et al. (2020). Higher than expected CO_2 fertilization inferred from leaf to global observations. *Global Change Biology*, *26*(4), 2390–2402. https://doi.org/10.1111/gcb.14950

Hedges, L. V., Gurevitch, J., & Curtis, P. S. (1999). The meta-analysis of response ratios in experimental ecology. *Ecology*, *80*(4), 1150–1156. https://doi.org/10.1890/0012-9658(1999)080[1150:TMAORR]2.0.CO;2

Hu, C., Liu, X., Driscoll, A. W., Kuang, Y., Brookshire, E., Lü, X., et al. (2024). Global distribution and drivers of relative contributions among soil nitrogen sources to terrestrial plants. *Nature Communications*, *15*(1), 6407. https://doi.org/10.1038/s41467-024-50674-6

Hu, Z., Piao, S., Knapp, A. K., Wang, X., Peng, S., Yuan, W., et al. (2022). Decoupling of greenness and gross primary productivity as aridity decreases. *Remote Sensing of Environment*, *279*, 113120. https://doi.org/10.1016/j.rse.2022.113120

Jiang, C., & Ryu, Y. (2016). Multi-scale evaluation of global gross primary productivity and evapotranspiration products derived from breathing earth system simulator (BESS). *Remote Sensing of Environment*, *186*, 528–547. https://doi.org/10.1016/j.rse.2016.08.030

Jung, M., Schwalm, C., Migliavacca, M., Walther, S., Camps-Valls, G., Koirala, S., et al. (2020). Scaling carbon fluxes from eddy covariance sites to globe: Synthesis and evaluation of the FLUXCOM approach. *Biogeosciences*, *17*(5), 1343–1365. https://doi.org/10.5194/bg-17-1343-2020

Kattge, J., Knorr, W., Raddatz, T., & Wirth, C. (2009). Quantifying photosynthetic capacity and its relationship to leaf nitrogen content for global-scale terrestrial biosphere models. *Global Change Biology*, *15*(4), 976–991. https://doi.org/10.1111/j.1365-2486.2008.01744.x

Keeling, C. D., & Whorf, T. P. (2005). Atmospheric CO_2 records from sites in the SIO air sampling network. In *Trends*: A compendium of data on global change (pp. 16–26).

Keenan, T. F., Luo, X., Stocker, B. D., De Kauwe, M. G., Medlyn, B. E., Prentice, I. C., et al. (2023). A constraint on historic growth in global photosynthesis due to rising CO_2. *Nature Climate Change*, *13*(12), 1376–1381. https://doi.org/10.1038/s41558-023-01867-2

Kovenock, M., & Swann, A. L. S. (2018). Leaf trait acclimation amplifies simulated climate warming in response to elevated carbon dioxide. *Global Biogeochemical Cycles*, *32*(10), 1437–1448. https://doi.org/10.1029/2018GB005883

Kowalczyk, E. A. (2006). The CSIRO atmosphere biosphere land exchange (CABLE) model for use in climate models and as an offline model. *CSIRO Marine and Atmospheric Research*, 013.

Lai, J., Kooijmans, L. M. J., Sun, W., Lombardozzi, D., Campbell, J. E., Gu, L., et al. (2024). Terrestrial photosynthesis inferred from plant carbonyl sulfide uptake. *Nature*, *634*(8035), 855–861. https://doi.org/10.1038/s41586-024-08050-3

Leakey, A. D., Ainsworth, E. A., Bernacchi, C. J., Rogers, A., Long, S. P., & Ort, D. R. (2009). Elevated CO_2 effects on plant carbon, nitrogen, and water relations: Six important lessons from FACE. *Journal of Experimental Botany*, *60*(10), 2859–2876. https://doi.org/10.1093/jxb/erp096

Lee, T. D., Barrott, S. H., & Reich, P. B. (2011). Photosynthetic responses of 13 grassland species across 11 years of free-air CO_2 enrichment is modest, consistent and independent of N supply. *Global Change Biology*, *17*(9), 2893–2904. https://doi.org/10.1111/j.1365-2486.2011.02435.x

Lei, L., Zhang, K., Zhang, X., Wang, Y. P., Xia, J., Piao, S., et al. (2019). Plant feedback aggravates soil organic carbon loss associated with wind erosion in northwest China. *Journal of Geophysical Research: Biogeosciences*, *124*(4), 825–839. https://doi.org/10.1029/2018JG004804

Leuning, R. (2002). Temperature dependence of two parameters in a photosynthesis model. *Plant, Cell & Environment*, *25*(9), 1205–1210. https://doi.org/10.1046/j.1365-3040.2002.00898.x

Leuning, R., Kelliher, F. M., De Pury, G., & Schulze, E. D. (1995). Leaf nitrogen, photosynthesis, conductance and transpiration: Scaling from leaves to canopies. *Plant, Cell & Environment*, *18*(10), 1183–1200. https://doi.org/10.1111/j.1365-3040.1995.tb00628.x

Li, Q., Lu, X., Wang, Y., Huang, X., Cox, P. M., & Luo, Y. (2018). Leaf area index identified as a major source of variability in modeled CO_2 fertilization. *Biogeosciences*, *15*(2), 6909–6925. https://doi.org/10.5194/bg-15-6909-2018

Lloret, F., Escudero, A., Iriondo, J. M., Martínez-Vilalta, J., & Valladares, F. (2012). Extreme climatic events and vegetation: The role of stabilizing processes. *Global Change Biology*, *18*(3), 797–805. https://doi.org/10.1111/j.1365-2486.2011.02624.x

Lu, X., Wang, Y. P., Wright, I. J., Reich, P. B., Shi, Z., & Dai, Y. (2017). Incorporation of plant traits in a land surface model helps explain the global biogeographical distribution of major forest functional types. *Global Ecology and Biogeography*, *26*(3), 304–317. https://doi.org/10.1111/geb.12535

Luo, Y., Field, C. B., & Mooney, H. A. (1994). Predicting responses of photosynthesis and root fraction to elevated [CO_2] A: Interactions among carbon, nitrogen, and growth. *Plant, Cell & Environment*, *17*(11), 1195–1204. https://doi.org/10.1111/j.1365-3040.1994.tb02017.x

21698961, 2026, 11, Downloaded from https://agupubs.onlinelibrary.wiley.com/doi/10.1029/2026JG010127 by Cornell University, Wiley Online Library on [06/11/2026]. See the Terms and Conditions (https://onlinelibrary.wiley.com/terms-and-conditions) on Wiley Online Library for rules of use; OA articles are governed by the applicable Creative Commons License

Madani, N., Kimball, J. S., & Running, S. W. (2017). Improving global gross primary productivity estimates by computing optimum light use efficiencies using flux tower data. *Journal of Geophysical Research-Biogeosciences*, *122*(11), 2939–2951. https://doi.org/10.1002/2017JG004142

Madani, N., Parazoo, N. C., Kimball, J. S., Ballantyne, A. P., Reichle, R. H., Maneta, M., et al. (2020). Recent amplified global gross primary productivity due to temperature increase is offset by reduced productivity due to water constraints. *AGU Advances*, *1*(4), e2020AV000180. https://doi.org/10.1029/2020AV000180

Mason, R. E., Craine, J. M., Lany, N. K., Jonard, M., Ollinger, S. V., Groffman, P. M., et al. (2022). Evidence, causes, and consequences of declining nitrogen availability in terrestrial ecosystems. *Science*, *376*(6590), eabh3767. https://www.science.org/doi/10.1126/science.abh3767

Medlyn, B. E., Zaehle, S., De Kauwe, M. G., Walker, A. P., Dietze, M. C., Hanson, P. J., et al. (2015). Using ecosystem experiments to improve vegetation models. *Nature Climate Change*, *5*(6), 528–534. https://doi.org/10.1038/nclimate2621

Nardini, A., Pedà, G., & La Rocca, N. (2012). Trade-offs between leaf hydraulic capacity and drought vulnerability: Morpho-anatomical bases, carbon costs and ecological consequences. *New Phytologist*, *196*(3), 788–798. https://doi.org/10.1111/j.1469-8137.2012.04294.x

Pastore, M. A., Lee, T. D., Hobbie, S. E., & Reich, P. B. (2019). Strong photosynthetic acclimation and enhanced water-use efficiency in grassland functional groups persist over 21 years of CO_2 enrichment, independent of nitrogen supply. *Global Change Biology*, *25*(9), 3031–3044. https://doi.org/10.1111/gcb.14714

Pedregosa, F., Varoquaux, G., Gramfort, A., Michel, V., Thirion, B., Grisel, O., et al. (2011). Scikit-learn: Machine learning in python. *Journal of Machine Learning Research*, *12*, 2825–2830.

Peterson, A. G., Ball, J. T., Luo, Y., Field, C. B., Reich, P. B., Curtis, P. S., et al. (1999). The photosynthesis-leaf nitrogen relationship at ambient and elevated atmospheric carbon dioxide: A meta-analysis. *Global Change Biology*, *5*(3), 331–346. https://doi.org/10.1046/j.1365-2486.1999.00234.x

Piao, S., Sitch, S., Ciais, P., Friedlingstein, P., Peylin, P., Wang, X., et al. (2013). Evaluation of terrestrial carbon cycle models for their response to climate variability and to CO_2 trends. *Global Change Biology*, *19*(7), 2117–2132. https://doi.org/10.1111/gcb.12187

Piao, S., Wang, X., Park, T., Chen, C., Lian, X., He, Y., et al. (2020). Characteristics, drivers and feedbacks of global greening. *Nature Reviews Earth & Environment*, *1*, 14–27. https://doi.org/10.1038/s43017-019-0001-x

Piao, S., Yin, G., Tan, J., Cheng, L., Huang, M., Li, Y., et al. (2015). Detection and attribution of vegetation greening trend in China over the last 30 years. *Global Change Biology*, *21*(4), 1601–1609. https://doi.org/10.1111/gcb.12795

Poorter, H., Knopf, O., Wright, I. J., Temme, A. A., Hogewoning, S. W., Graf, A., et al. (2022). A meta-analysis of responses of C3 plants to atmospheric CO_2: Dose–response curves for 85 traits ranging from the molecular to the whole-plant level. *New Phytologist*, *233*(4), 1560–1596. https://doi.org/10.1111/nph.17802

Poorter, H., Niinemets, Ü., Poorter, L., Wright, I. J., & Villar, R. (2009). Causes and consequences of variation in leaf mass per area (LMA): A meta-analysis. *New Phytologist*, *182*(3), 565–588. https://doi.org/10.1111/j.1469-8137.2009.02830.x

Poorter, H., Van Berkel, Y., Baxter, R., Den Hertog, J., Dijkstra, P., Gifford, R. M., et al. (1997). The effect of elevated CO_2 on the chemical composition and construction costs of leaves of 27 C3 species. *Plant, Cell and Environment*, *20*(4), 472–482. https://doi.org/10.1046/j.1365-3040.1997.d01-84.x

Randerson, J. T., Li, Y., Fu, W., Primeau, F., Kim, J. E., Mu, M., et al. (2025). The weak land carbon sink hypothesis. *Science Advances*, *11*(37), eadr5489. https://doi.org/10.1126/sciadv.adr5489

Reich, P. B. (2012). Key canopy traits drive forest productivity. *Proceedings of the Royal Society B: Biological Sciences*, *279*(1736), 2128–2134. https://doi.org/10.1098/rspb.2011.2270

Reich, P. B. (2014). The world-wide 'fast-slow' plant economics spectrum: A traits manifesto. *Journal of Ecology*, *102*(2), 275–301. https://doi.org/10.1111/1365-2745.12211

Reich, P. B., Ellsworth, D. S., & Walters, M. B. (1998). Leaf structure (specific leaf area) modulates photosynthesis–nitrogen relations: Evidence from within and across species and functional groups. *Functional Ecology*, *12*(6), 948–958. https://doi.org/10.1046/j.1365-2435.1998.00274.x

Reich, P. B., Walters, M. B., & Ellsworth, D. S. (1997). From tropics to tundra: Global convergence in plant functioning. *Proceedings of the National Academy of Sciences*, *94*(25), 13730–13734. https://doi.org/10.1073/pnas.94.25.13730

Rogers, A. (2014). The use and misuse of vc,max in Earth system models. *Photosynthesis Research*, *119*(1–2), 15–29. https://doi.org/10.1007/s11120-013-9818-1

Rosas, T., Mencuccini, M., Barba, J., Cochard, H., Saura-Mas, S., & Martínez-Vilalta, J. (2019). Adjustments and coordination of hydraulic, leaf and stem traits along a water availability gradient. *New Phytologist*, *223*(2), 632–646. https://doi.org/10.1111/nph.15684

Ryu, Y., Berry, J. A., & Baldocchi, D. D. (2019). What is global photosynthesis? History, uncertainties and opportunities. *Remote Sensing of Environment*, *223*, 95–114. https://doi.org/10.1016/j.rse.2019.01.016

Sage, R. F. (1990). A model describing the regulation of ribulose-1, 5-bisphosphate carboxylase, electron transport, and triose phosphate use in response to light intensity and CO_2 in C3 plants. *Plant Physiology*, *94*(4), 1728–1734. https://doi.org/10.1104/pp.94.4.1728

Schäfer, K. V. R., Oren, R., Ellsworth, D. S., Lai, C.-T., Herrick, J. D., Finzi, A. C., et al. (2003). Exposure to an enriched CO_2 atmosphere alters carbon assimilation and allocation in a pine forest ecosystem. *Global Change Biology*, *9*(10), 1378–1400. https://doi.org/10.1046/j.1365-2486.2003.00662.x

Smith, N. G., & Dukes, J. S. (2013). Plant respiration and photosynthesis in global-scale models: Incorporating acclimation to temperature and CO_2. *Global Change Biology*, *19*(1), 45–63. https://doi.org/10.1111/j.1365-2486.2012.02797.x

Smith, N. G., & Keenan, T. F. (2020). Mechanisms underlying leaf photosynthetic acclimation to warming and elevated CO_2 as inferred from least-cost optimality theory. *Global Change Biology*, *26*(9), 5202–5216. https://doi.org/10.1111/gcb.15212

Smith, N. G., Zhu, Q., Keenan, T. F., & Riley, W. J. (2024). Acclimation of photosynthesis to CO_2 increases ecosystem carbon storage due to leaf nitrogen savings. *Global Change Biology*, *30*(11), e17558. https://doi.org/10.1111/gcb.17558

Stevens, N., Lehmann, C. E. R., Murphy, B. P., & Durigan, G. (2017). Savanna woody encroachment is widespread across three continents. *Global Change Biology*, *23*(1), 235–244. https://doi.org/10.1111/gcb.13409

Stocker, B. D., Dong, N., Perkowski, E. A., Schneider, P. D., Xu, H., de Boer, H. J., et al. (2025). Empirical evidence and theoretical understanding of ecosystem carbon and nitrogen cycle interactions. *New Phytologist*, *245*(1), 49–68. https://doi.org/10.1111/nph.20178

Tietjen, B., Schlaepfer, D. R., Bradford, J. B., Lauenroth, W. K., Hall, S. A., Duniway, M. C., et al. (2017). Climate change-induced vegetation shifts lead to more ecological droughts despite projected rainfall increases in many global temperate drylands. *Global Change Biology*, *23*(7), 2743–2754. https://doi.org/10.1111/gcb.13598

Trabucco, A., & Zomer, R. (2019). Global aridity index and potential evapotranspiration (ET0) database: Version 3. [Dataset]. *Figshare*. https://doi.org/10.6084/m9.figshare.7504448.v5

UNEP. (1997). *World atlas of desertification* (2nd ed. vol. SECOND EDITION). United Nations Environment Program.

21698961, 2026, 11, Downloaded from https://agupubs.onlinelibrary.wiley.com/doi/10.1029/2026JG010127 by Cornell University, Wiley Online Library on [06/11/2026]. See the Terms and Conditions (https://onlinelibrary.wiley.com/terms-and-conditions) on Wiley Online Library for rules of use; OA articles are governed by the applicable Creative Commons License

Van Bodegom, P. M., Douma, J. C., Witte, J. P. M., Ordoñez, J. C., Bartholomeus, R. P., & Aerts, R. (2012). Going beyond limitations of plant functional types when predicting global ecosystem-atmosphere fluxes: Exploring the merits of traits-based approaches. *Global Ecology and Biogeography*, *21*(6), 625–636. https://doi.org/10.1111/j.1466-8238.2011.00717.x

Viovy, N. (2018). CRUNCEP version 7-Atmospheric forcing data for the community land model. NSF national center for atmospheric research [Dataset]. *GDEX*. https://doi.org/10.5065/PZ8F-F017

Walker, A. P., De Kauwe, M. G., Bastos, A., Belmecheri, S., Georgiou, K., Keeling, R. F., et al. (2021). Integrating the evidence for a terrestrial carbon sink caused by increasing atmospheric CO_2. *New Phytologist*, *229*(5), 2413–2445. https://doi.org/10.1111/nph.16866

Walker, X. J., Baltzer, J. L., Cumming, S. G., Day, N. J., Ebert, C., Goetz, S., et al. (2019). Increasing wildfires threaten historic carbon sink of boreal forest soils. *Nature*, *572*(7770), 520–523. https://doi.org/10.1038/s41586-019-1474-y

Wang, H., Prentice, I. C., Keenan, T. F., Davis, T. W., Wright, I. J., Cornwell, W. K., et al. (2017). Towards a universal model for carbon dioxide uptake by plants. *Nature Plants*, *3*(9), 734–741. https://doi.org/10.1038/s41477-017-0006-8

Wang, L. (2024). Global plant nitrogen use is controlled by temperature. *Nature Communications*, *15*(1), 7651. https://doi.org/10.1038/s41467-024-50803-1

Wang, Y.-P., Houlton, B. Z., & Field, C. B. (2007). A model of biogeochemical cycles of carbon, nitrogen, and phosphorus including symbiotic nitrogen fixation and phosphatase production. *Global Biogeochemical Cycles*, *21*(1), 1. https://doi.org/10.1029/2006GB002797

Wang, Y.-P., Kowalczyk, E., Leuning, R., Abramowitz, G., Raupach, M. R., Pak, B., et al. (2011). Diagnosing errors in a land surface model (CABLE) in the time and frequency domains. *Journal of Geophysical Research*, *116*(G1), G01034. https://doi.org/10.1029/2010JG001385

Wang, Y.-P., Law, R. M., & Pak, B. (2010). A global model of carbon, nitrogen and phosphorus cycles for the terrestrial biosphere. *Biogeosciences*, *7*(7), 2261–2282. https://doi.org/10.5194/bg-7-2261-2010

Wang, Y.-P., & Leuning, R. (1998). A two-leaf model for canopy conductance, photosynthesis and partitioning of available energy I: Model description and comparison with a multi-layered model. *Agricultural and Forest Meteorology*, *91*(1–2), 89–111. https://doi.org/10.1016/S0168-1923(98)00061-6

Wang, Y.-P., Lu, X., Wright, I. J., Dai, Y., Rayner, P. J., & Reich, P. B. (2012). Correlations among leaf traits provide a significant constraint on the estimate of global gross primary production. *Geophysical Research Letters*, *39*(19), L19405. https://doi.org/10.1029/2012GL053461

Wei, N., Xia, J., Wang, Y.-P., Zhang, X., Zhou, J., Bian, C., & Luo, Y. (2022). Nutrient limitations lead to a reduced magnitude of disequilibrium in the global terrestrial carbon cycle. *Journal of Geophysical Research-Biogeosciences*, *127*(5), e2021JG006764. https://doi.org/10.1029/2021JG006764

Welp, L. R., Keeling, R. F., Meijer, H. A. J., Bollenbacher, A. F., Piper, S. C., Yoshimura, K., et al. (2011). Interannual variability in the oxygen isotopes of atmospheric CO_2 driven by El Niño. *Nature*, *477*(7366), 579–582. https://doi.org/10.1038/nature10421

Westerband, A. C., Wright, I. J., Maire, V., Paillassa, J., Prentice, I. C., Atkin, O. K., et al. (2023). Coordination of photosynthetic traits across soil and climate gradients. *Global Change Biology*, *29*(3), 856–873. https://doi.org/10.1111/gcb.16501

Wright, I. J., Reich, P. B., Cornelissen, J. H. C., Falster, D. S., Garnier, E., Hikosaka, K., et al. (2005). Assessing the generality of global leaf trait relationships. *New Phytologist*, *166*(2), 485–496. https://doi.org/10.1111/j.1469-8137.2005.01349.x

Wright, I. J., Reich, P. B., Cornelissen, J. H. C., Falster, D. S., Groom, P. K., Hikosaka, K., et al. (2005). Modulation of leaf economic traits and trait relationships by climate. *Global Ecology and Biogeography*, *14*(5), 411–421. https://doi.org/10.1111/j.1466-822x.2005.00172.x

Wright, I. J., & Westoby, M. (2002). Leaves at low versus high rainfall: Coordination of structure, lifespan and physiology. *New Phytologist*, *155*(3), 403–416. https://doi.org/10.1046/j.1469-8137.2002.00479.x

Wright, I. J., Westoby, M., Ackerly, D. D., Baruch, Z., Bongers, F., Cavender-Bares, J., et al. (2004). The worldwide leaf economics spectrum. *Nature*, *428*(6985), 821–827. https://doi.org/10.1038/nature02403

Xia, J., Luo, Y., Wang, Y.-P., Weng, E., & Hararuk, O. (2012). A semi-analytical solution to accelerate spin-up of a coupled carbon and nitrogen land model to steady state. *Geoscientific Model Development*, *5*(5), 1259–1271. https://doi.org/10.5194/gmd-5-1259-2012

Yang, J., Medlyn, B. E., De Kauwe, M. G., Duursma, R. A., Jiang, M., Kumarathunge, D., et al. (2020). Low sensitivity of gross primary production to elevated CO_2 in a mature eucalypt woodland. *Biogeosciences*, *17*(2), 265–279. https://doi.org/10.5194/bg-17-265-2020

Yang, Y., Roderick, M. L., Zhang, S., McVicar, T. R., & Donohue, R. J. (2019). Hydrologic implications of vegetation response to elevated CO_2 in climate projections. *Nature Climate Change*, *9*(1), 44–48. https://doi.org/10.1038/s41558-018-0361-0

Yuan, W., Liu, S., Yu, G., Bonnefond, J., Chen, J., Davis, K., et al. (2010). Global estimates of evapotranspiration and gross primary production based on MODIS and global meteorology data. *Remote Sensing of Environment*, *114*(7), 1416–1431. https://doi.org/10.1016/j.rse.2010.01.022

Yuan, W., Zheng, Y., Piao, S., Ciais, P., Lombardozzi, D., Wang, Y., et al. (2019). Increased atmospheric vapor pressure deficit reduces global vegetation growth. *Science Advances*, *5*(8), eaax1396. https://doi.org/10.1126/sciadv.aax1396

Zaehle, S., Medlyn, B. E., De Kauwe, M. G., Walker, A. P., Dietze, M. C., Hickler, T., et al. (2014). Evaluation of 11 terrestrial carbon-nitrogen cycle models against observations from two temperate free-air CO_2 enrichment studies. *New Phytologist*, *202*(3), 803–822. https://doi.org/10.1111/nph.12697

Zeng, Z., Piao, S., Li, Z., Zhou, L., Ciais, P., Wang, T., et al. (2017). Climate mitigation from vegetation biophysical feedbacks during the past three decades. *Nature Climate Change*, *7*(6), 432–436. https://doi.org/10.1038/nclimate3299

Zhang, X., Rayner, P. J., Wang, Y.-P., Silver, J. D., Lu, X., Pak, B., & Zheng, X. (2016). Linear and nonlinear effects of dominant drivers on the trends in global and regional land carbon uptake: 1959 to 2013. *Geophysical Research Letters*, *43*(4), 1607–1614. https://doi.org/10.1002/2015GL067162

Zaehle, S., & Friend, A. D. (2010). Carbon and nitrogen cycle dynamics in the O-CN land surface model: 1. Model description, site-scale evaluation, and sensitivity to parameter estimates. *Global Biogeochemical Cycles*, *24*(1), GB1005. https://doi.org/10.1029/2009GB003521

Zhou, J., Cieraad, E., & van Bodegom, P. M. (2022). Global analysis of trait–trait relationships within and between species. *New Phytologist*, *233*(4), 1643–1656. https://doi.org/10.1111/nph.17879

Zomer, R. J., Xu, J., & Trabucco, A. (2022). Version 3 of the global aridity index and potential evapotranspiration database. *Scientific Data*, *9*(1), 409. https://doi.org/10.1038/s41597-022-01493-1

References From the Supporting Information

Biome-BGC. (2010). Biome BGC version 4.2: Theoretical framework of BIOME-BGC. Retrieved from http://www.ntsg.umt.edu/project/biome-bgc

Chen, Z., Wang, W., Forzieri, G., & Cescatti, A. (2024). Transition from positive to negative indirect CO_2 effects on the vegetation carbon uptake. *Nature Communications*, *15*(1), 1500. https://doi.org/10.1038/s41467-024-45957-x

21698961, 2026, 11, Downloaded from https://agupubs.onlinelibrary.wiley.com/doi/10.1029/2026JG010127 by Cornell University, Wiley Online Library on [06/11/2026]. See the Terms and Conditions (https://onlinelibrary.wiley.com/terms-and-conditions) on Wiley Online Library for rules of use; OA articles are governed by the applicable Creative Commons License

Ciais, P., Tagliabue, A., Cuntz, M., Bopp, L., Scholze, M., Hoffmann, G., et al. (2012). Large inert carbon pool in the terrestrial biosphere during the last glacial maximum. *Nature Geoscience*, *5*(1), 74–79. https://doi.org/10.1038/ngeo1324

Clark, D. B., Mercado, L. M., Sitch, S., Jones, C. D., Gedney, N., Best, M. J., et al. (2011). The joint UK land environment simulator (JULES), model description–part 2: Carbon fluxes and vegetation dynamics. *Geoscientific Model Development*, *4*(3), 701–722. https://doi.org/10.5194/gmd-4-701-2011

Davies, R. B. (1987). Hypothesis testing when a nuisance parameter is present only under the alternative. *Biometrika*, *74*(1), 33–43. https://doi.org/10.1093/biomet/74.1.33

Friend, A. D. (2010). Terrestrial plant production and climate change. *Journal of Experimental Botany*, *61*(5), 1293–1309. https://doi.org/10.1093/jxb/erq019

Kolby Smith, W., Reed, S. C., Cleveland, C. C., Ballantyne, A. P., Anderegg, W. R., Wieder, W. R., et al. (2016). Large divergence of satellite and Earth system model estimates of global terrestrial CO_2 fertilization. *Nature Climate Change*, *6*(3), 306–310. https://doi.org/10.1038/nclimate2879

Muggeo, V. M. (2008). Segmented: An R package to fit regression models with broken-line relationships. *R News*, *8*, 20–25.

Oleson, K. W., Lawrence, D. M., Bonan, G. B., Fisher, R. A., Lawrence, P. J., & Muszala, S. P. (2013). Technical description of version 4.5 of the community land model (CLM). *National Center for Atmospheric Research Technical Note*, *503*. https://doi.org/10.5065/D6RR1W7M

Oleson, K. W., Lawrence, D. M., Bonan, G. B., Flanner, M. G., Kluzek, E., Lawrence, P. J., et al. (2010). Technical description of version 4.0 of the community land model (CLM). *National Center for Atmospheric Research Technical Note*.

Raddatz, T. J., Reick, C. H., Knorr, W., Kattge, J., Roeckner, E., Schnur, R., et al. (2007). Will the tropical land biosphere dominate the climate–carbon cycle feedback during the twenty-first century? *Climate Dynamics*, *29*(6), 565–574. https://doi.org/10.1007/s00382-007-0247-8

Toms, J. D., & Lesperance, M. L. (2003). Piecewise regression: A tool for identifying ecological thresholds. *Ecology*, *84*(8), 2034–2041. https://doi.org/10.1890/02-0472

Wang, S., Zhang, Y., Ju, W., Chen, J. M., Ciais, P., Cescatti, A., et al. (2020). Recent global decline of CO_2 fertilization effects on vegetation photosynthesis. *Science*, *370*(6522), 1295–1300. https://doi.org/10.1126/science.abb7772

Walker, A. P., Beckerman, A. P., Gu, L., Kattge, J., Cernusak, L. A., Domingues, T. F., et al. (2014). The relationship of leaf photosynthetic traits-Vcmax and Jmax-to leaf nitrogen, leaf phosphorus, and specific leaf area: A meta-analysis and modeling study. *Ecology and Evolution*, *4*(16), 3218–3235. https://doi.org/10.1002/ece3.1173

Zhu, Q., Riley, W. J., Tang, J., Collier, N., Hoffman, F. M., Yang, X., & Bisht, G. (2019). Representing nitrogen, phosphorus, and carbon interactions in the E3SM land model: Development and global benchmarking. *Journal of Advances in Modeling Earth Systems*, *11*(7), 2238–2258. https://doi.org/10.1029/2018MS001571

Ziehn, T., Kattge, J., Knorr, W., & Scholze, M. (2011). Improving the predictability of global CO_2 assimilation rates under climate change. *Geophysical Research Letters*, *38*(10), 1513–1531. https://doi.org/10.1029/2011GL047182

21698961, 2026, 11, Downloaded from https://agupubs.onlinelibrary.wiley.com/doi/10.1029/2026JG010127 by Cornell University, Wiley Online Library on [06/11/2026]. See the Terms and Conditions (https://onlinelibrary.wiley.com/terms-and-conditions) on Wiley Online Library for rules of use; OA articles are governed by the applicable Creative Commons License